nature chemistry

SUPPLEMENTARY INFORMATION

DOI: 10.1038/NCHEM.479

Radically Enhanced Molecular Recognition

Ali Trabolsi[1,2], Niveen Khashab[1,2], Albert C. Fahrenbach[1], Douglas C. Friedman[1], Michael T. Colvin[3], Karla Cotí[1,4], Diego Benítez[5], Ekaterina Tkatchouk[5], John-Carl Olsen[1,4], Matthew E. Belowich[1], Raanan Carmielli[3], Hussam A. Khatib[1,2], William A. Goddard III[5], Michael R. Wasielewski[3], and J. Fraser Stoddart[1*]

[1]Department of Chemistry, Northwestern University, 2145 Sheridan Road, Evanston, IL 60208, USA. [2]Current location King Abdullah University of Science and Technology (KAUST), Thuwal, KSA. [3]Department of Chemistry, Argonne-Northwestern Solar Energy Research (ANSER) Center, and International Institute for Nanotechnology, Northwestern University [4]Department of Chemistry and Biochemistry, University of California, Los Angeles, CA 90095, USA. [5]Materials and Process Simulation Center, California Institute of Technology, Pasadena, CA 91125, USA. *e-mail: stoddart@northwestern.edu.

1. General Methods

All reagents were purchased from commercial suppliers (Aldrich or Fisher) and used without further purification. Cyclobis(paraquat-*p*-phenylene) tetrakis(hexafluorophosphate)[S1] (**CBPQT**·4PF_6), the bisalkyne viologen[S2] **V**·2PF_6, 2-(2-(2,6-diisopropylphenoxy)ethoxy)ethyl-4-methylbenzene-sulfonate[S3,S4,S5] (**S1**), 1,5-bis[2-(2-hydroxyethoxy)ethoxy)] naphthalene[S6] and its monotosyl derivative[S7] **S3**, and tris(benzyltriazolylmethyl)amine (TBTA) [S8] were prepared according to literature procedures. Thin layer chromatography (TLC) was performed on silica gel 60 F254 (E. Merck). Column chromatography was performed on silica gel 60F (Merck 9385, 0.040–0.063 mm). Routine nuclear magnetic resonance (NMR) spectra were recorded at 25 °C on a Bruker Avance 600 and Varian Inova 500 spectrometers, with working frequencies of 600 and 500 MHz for ^{1}H, and 150 and 125 MHz for ^{13}C nuclei, respectively. Chemical shifts are reported in ppm relative to the signals corresponding to the residual non-deuterated solvents ($CDCl_3$: δ 7.26 ppm, CD_3CN: δ 1.94 ppm, CD_3COCD_3: δ 2.05 ppm). All ^{13}C spectra were recorded with the simultaneous decoupling of proton nuclei. High-resolution mass spectra were

measured, either on an Applied Biosystems Voyager DE-PRO MALDI TOF mass spectrometer (HR-TOF), or on a Finnigan LCQ iontrap mass spectrometer (HR-ESI). Cyclic voltammetry experiments (CV) and spectroelectrochemical (SEC) experiments were carried out at room temperature in argon-purged solutions in MeCN with a Gamry Multipurpose instrument (Reference 600) interfaced to a PC. CV experiments were performed using a glassy carbon working electrode (0.018 cm^2, Cypress system). The electrode surface was polished routinely with a 0.05 μm alumina-water slurry on a felt surface immediately before use. The counter electrode was a Pt coil and the reference electrode was a Ag/AgCl electrode. The concentration of the sample and supporting electrolyte tetrabutylammonium hexafluorophosphate ($TBAPF_6$) were 1.0×10^{-3} mol L^{-1} and 0.1 mol L^{-1}, respectively. The scan rate was set to 200 mV s^{-1}. SEC experiments were carried out using a custom-built optically-transparent thin-layer electrochemical (OTTLE) cell with an optical path of 1 mm, using a Pt grid as working electrode, a Pt wire as counter electrode and a Ag wire pseudo-reference electrode. Experimental errors: potential values, +/– 10 mV, absorption maxima, +/– 1 nm. UV/Vis Spectra were recorded at room temperature on a Varian 100 Bio-instrument.

2. Synthesis

S2: The tosylate **S1**[S9] (2g, 4.75 mmol) and NaN_3 (618 mg, 9.5 mmol) were dissolved in dry DMF (25 mL). The mixture was then stirred at 80 °C for 16 h. After cooling down to room temperature, the solvent was removed in vacuo, and the crude material was filtered through a pad of silica, eluting with Me_2CO. A pure yellow oil (1.36 g, 98 %) of **S2** was obtained. ^{1}H NMR (500 MHz, $CDCl_3$): δ = 7.09 (br s, 3H), 3.93 (t, *J* = 4 Hz, 2H), 3.86 (t, *J* = 4 Hz, 2H), 3.78 (t, *J* = 4 Hz, 2H), 3.45 (t, *J* = 4 Hz, 2H), 3.38 (septet, *J* = 7 Hz, 2H), 1.22 (d, *J* = 7 Hz, 12 H). ^{13}C NMR (125 MHz, $CDCl_3$): δ =152.8, 141.8, 124.7, 124.1, 73.9, 70.6, 70.4, 50.9, 26.7, 24.1. MS (ESI): *m/z* Calcd for $C_{16}H_{26}N_3O_2$: 292.39, found: 292.20 $[M + H]^+$.

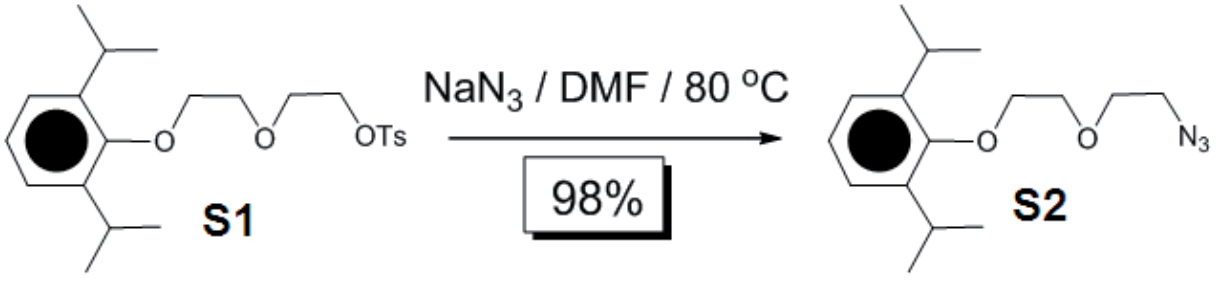

Scheme S1. Synthesis of the azide derivative **S2**

SV·2PF_6: Compounds **S2** (326 mg, 1.116 mmol) and **V**·2PF_6 (205 mg, 0.372 mmol) were mixed in Me_2CO (50 mL). A catalytic amount of tetrakis(acetonitrile)-copper(I) hexafluorophosphate ($Cu(MeCN)_4PF_6$) and TBTA were added at room temperature, and the mixture was left to stir overnight. After the removal of the solvent by evaporation, the residue was redissolved in a minimal amount of Me_2CO, and a saturated aqueous solution of EDTA at pH 8 was added. Addition of ammonium hexafluorophosphate resulted in the formation of a precipitate, which was collected by filtration, before being further purified by column chromatography (SiO_2, Me_2CO plus 2% ammonium hexafluorophosphate). Concentration in vacuo afforded the fully stoppered viologen **SV**·2PF_6 in 74% yield (312 mg) as a yellow oil. ^{1}H NMR (500 MHz, CD_3COCD_3): δ = 9.36 (d, *J* = 7 Hz, 4H), 8.78 (d, *J* = 7 Hz, 4H), 9.89 (s, 2H), 7.07 (m, 3H), 5.26 (t, *J* = 6 Hz, 4H), 4.58 (t, *J* = 5 Hz, 4H), 3.95 (t, *J* = 5 Hz, 4H), 3.85 (m, 4H), 3.80 (m, 4H), 3.58 (t, *J* = 7 Hz, 4H), 3.36 (septet, *J* = 7 Hz, 4H), 1.13 (d, *J* = 7 Hz, 24 H). ^{13}C (125 MHz, CD_3COCD_3): δ = 153.8, 150.9 ,147.2, 142.4, 142.3, 127.8, 125.5, 124.8, 124.3, 74.7, 71.0, 70.2, 66.0, 62.1, 26.7, 24.3. HRMS (HR-ESI): *m/z* Calcd for $C_{50}H_{67}F_6N_8O_4P$: 989.50, found: 989.50058 $[M - PF_6]^+$. *m/z* Calcd for $C_{50}H_{67}N_8O_4$: 422.27, found: 422.26806 $[M - 2PF_6]^{2+}$.

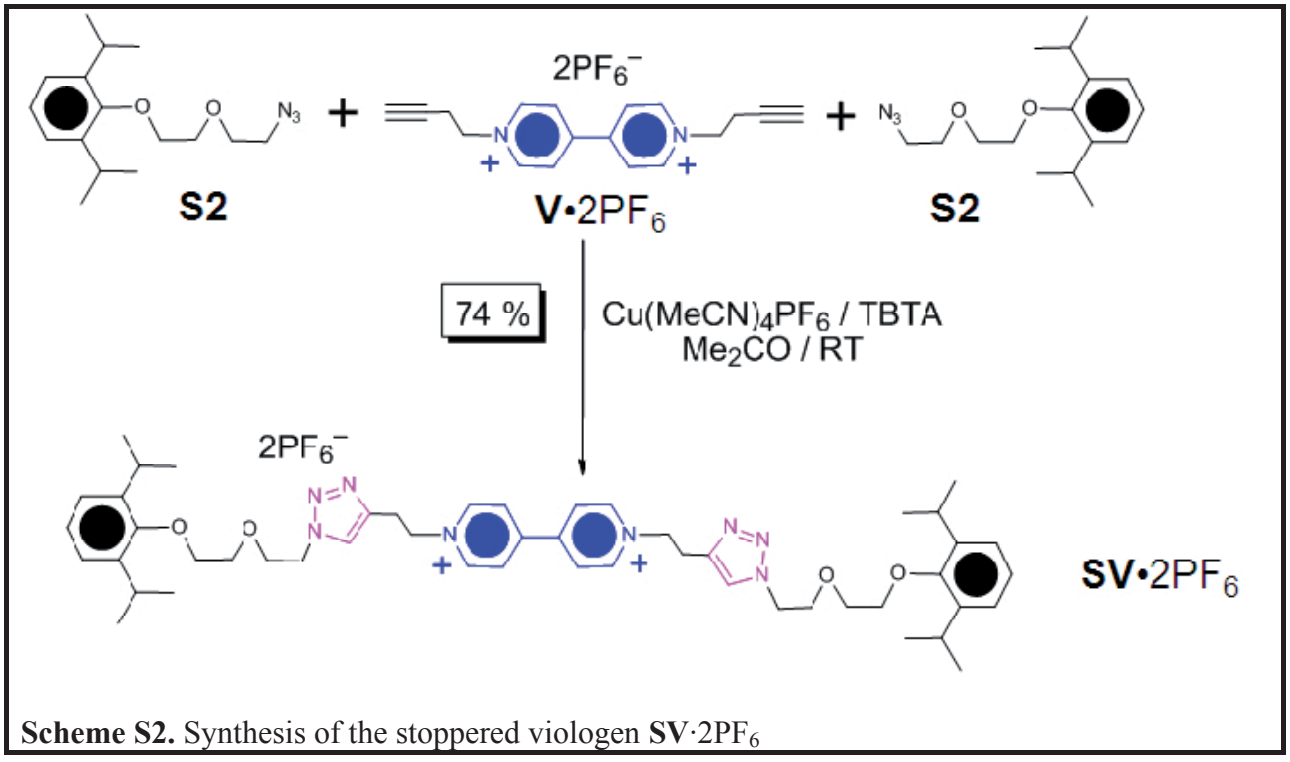

Scheme S2. Synthesis of the stoppered viologen **SV**·2PF_6

MSV·2PF_6: A solution (10 mL) of the azide **S2** (105.8 mg, 0.36 mmol) in Me_2CO was added dropwise at room temperature over 2 h to a solution of the bisalkyneviologen **V**·2PF_6 (400 mg, 0.72 mmol) containing a catalytic amount of tris(benzyltriazolylmethyl)amine (TBTA) and tetrakis(acetonitrile)copper(I) hexafluorophosphate. The reaction mixture was left to stand overnight. After removal of the solvent by evaporation, the residue was redissolved in a minimal amount of Me_2CO, and a saturated aqueous solution of EDTA (pH 8) was added. Addition of NH_4PF_6 resulted in a precipitate, which was collected by filtration and further purified by column chromatography (SiO_2, Me_2CO plus 2% NH_4PF_6). Concentration of the relevant fractions under vacuum afforded the viologen derivative **MSV**·2PF_6 in 65% yield (197 mg) as yellow oil. ^{1}H NMR (500 MHz, CD_3COCD_3): δ = 9.43 (d, *J* = 7.2 Hz, 2H), 9.35 (d, *J* = 6.1 Hz, 2H), 8.84 (d, *J* = 7.2 Hz, 2H), 8.78 (d, *J* = 6.1 Hz, 2H), 7.89 (s, 1H), 7.07 (m, 3H), 5.25 (t, *J* = 6.3 Hz, 2H), 5.09 (t, *J* = 6.3 Hz, 2H), 4.58 (t, *J* = 5.2 Hz, 2H), 3.96 (t, *J* = 5.2 Hz, 2H), 3.85 (m, 2H), 3.8 (m, 2H), 3.59 (t, *J* = 6.3 Hz, 2H), 3.39 (septet, *J* = 6.6 Hz, 2H), 3.15 (doublet of triplet, J_t = 6.3Hz, J_d = 2.4 Hz, 2H), 2.67 (t, *J* = 2.4 Hz, 1H), 1.13 (d, *J* = 6.6 Hz, 12 H). ^{13}C NMR (125 MHz, CD_3COCD_3): δ=154.2, 151.7, 151.3, 147.6, 147.5, 142.8, 128.3, 128.2, 125.9, 125.1, 79.4, 75.4, 75.1, 71.3, 70.5, 62.5, 61.3, 55.3, 51.2, 28.2, 27.1, 24.7, 21.9. MS (ESI): *m/z* Calcd for $C_{34}H_{43}F_6N_5O_2P$: 698.31, found 698.3 $[M - PF_6]^+$. *m/z* Calcd for $C_{34}H_{43}N_5O_2$: 276.67, found 276.7 $[M - 2PF_6]^{2+}$.

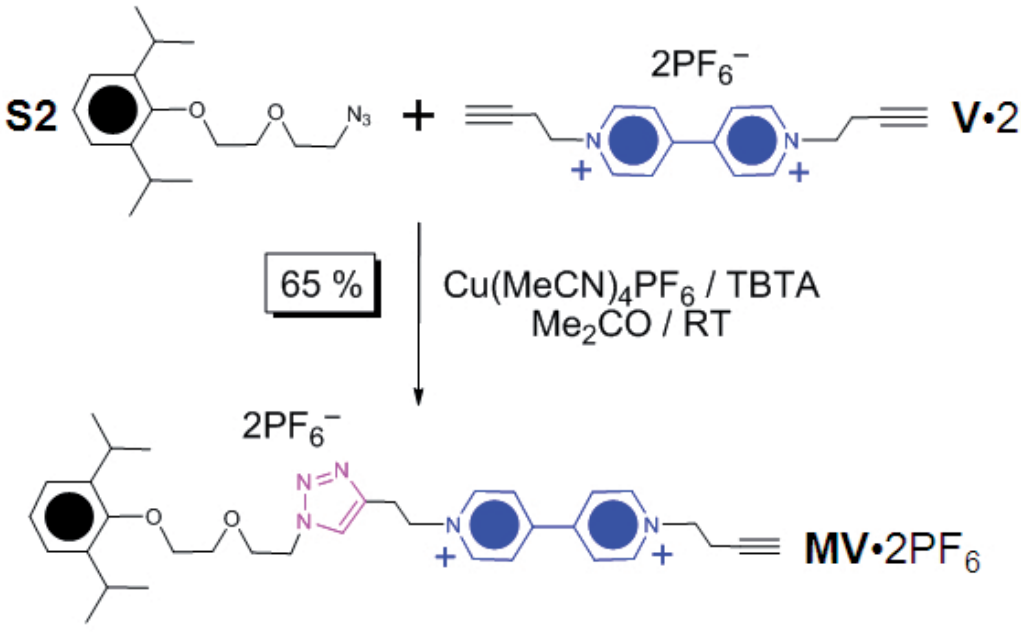

Scheme S3. Synthesis of the viologen derivative **MSV**·2PF_6

S4: A solution of monotosylate **S3** (1.2 g, 2.45 mmol), diisopropylphenol (524.14 mg, 2.94 mmol) and 10 equiv of K_2CO_3 were dissolved in anhydrous MeCN (80 mL) and the solution was heated under reflux for 20 h. After cooling down to room temperature, the solvent was evaporated, extracted with CH_2Cl_2, and washed with H_2O. The solvent was then evaporated and the remaining residue was purified by column chromatography (SiO_2: EtOAc) to afford **S4** as a viscous yellow oil in 95% yield (1.15 g). ^{1}H NMR (500 MHz, $CDCl_3$): δ = 7.98 (d, *J* = 8.5 Hz, 2H), 7.93 (d, *J* = 8.5 Hz, 2H), 7.44–7.39 (m, 2H), 7.18–7.12 (m, 3H), 6.93 (d, *J* = 8 Hz, 1H), 6.88 (d, *J* = 8 Hz, 1H), 4.39 (t, *J* = 4.5 Hz, 2H), 4.31 (t, *J* = 4.5 Hz, 2H), 4.14 (t, *J* = 4.5 Hz, 2H), 4.07–3.99 (m, 6H), 3.80 (t, *J* = 4.5 Hz, 2H), 3.75 (t, *J* = 4.5 Hz, 2H), 3.48 (m, *J* = 6.5 Hz, 2H), 1.27 (d, *J* = 7 Hz, 12 H). ^{13}C NMR (125 MHz, $CDCl_3$): δ = 154.7, 154.5, 153.3, 142.1, 127.1, 127.0, 125.5, 125.3, 124.9, 124.3, 115.1, 114.8, 106.0, 74.3, 72.9, 71.1, 70.3, 70.0, 68.4, 68.1, 62.1, 62.0. MS (ESI): *m/z* Calcd for $C_{30}H_{41}O_6$: 497.28, found 497.20 $[M + H]^+$.

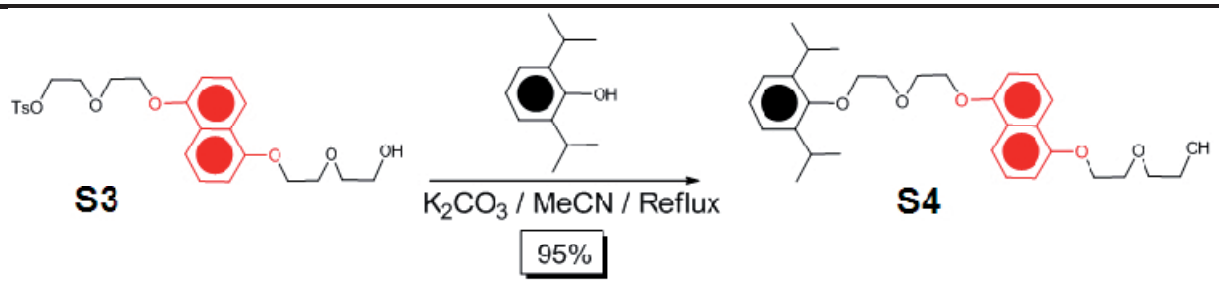

Scheme S4. Synthesis of DNP derivative **S4**

S5: The alcohol **S4** (1.38 g, 2.77 mmol), NEt_3 (555 mg, 780 µL, 5.50 mmol), and DMAP (20 mg, 0.16 mmol) were dissolved in CH_2Cl_2 (50 mL). A solution of tosyl chloride (525 mg, 2.71 mmol) in CH_2Cl_2 (18 mL) was added dropwise (syringe pump, 1.5 mL/h) to this mixture over 12 h at 23 °C. After the addition was complete, the reaction mixture was left to stir at 23 °C for an additional 4 h. The reaction mixture was then washed with saturated aqueous $NaHCO_3$ and then brine and dried ($MgSO_4$). The solvent was evaporated and the residue was purified by column chromatography (SiO_2: EtOAc) to afford **S5** as a viscous yellow oil in 98% yield (1.77 g). ^{1}H NMR (500 MHz, $CDCl_3$): δ = 7.99 (d, *J* = 8.5 Hz, 1H), 7.89 (d, *J* = 8.5 Hz, 1H), 7.82 (d, *J* = 8.5 Hz, 2H), 7.41 (m, 2H), 7.25 (d, *J* = 8.5 Hz, 2H), 7.18–7.12 (m, 3H), 6.94 (d, *J* = 8.5 Hz, 1H), 6.84 (d, *J* = 8.5 Hz, 1H), 4.40 (t, *J* = 4.5 Hz, 2H), 4.25 (t, *J* = 4.5 Hz, 2H), 4.21 (t, *J* = 4.5 Hz, 2H), 4.15 (t, *J* = 4.5 Hz, 2H), 4.05–4.03 (m, 4H), 3.92 (t, *J* = 4.5 Hz, 2H), 3.84 (t, *J* = 4.5 Hz,

2H), 3.49 (m, J = 7.0 Hz, 2H), 2.37 (s, 3H), 1.28 (d, J = 7.0 Hz, 12H). ^{13}C NMR (125 MHz, $CDCl_3$): δ = 154.7, 154.5, 153.3, 145.0, 142.1, 133.2, 130.0, 128.2, 127.1, 127.0, 125.5, 125.4, 124.9, 124.3, 115.0, 114.8, 106.1, 105.9, 74.3, 71.2, 70.3, 70.1, 69.7, 69.2, 68.4, 68.1, 26.5, 24.4, 21.8. MS (ESI): *m/z* Calcd for $C_{37}H_{47}O_8S$: 651.29, found 651.20 $[M + H]^+$.

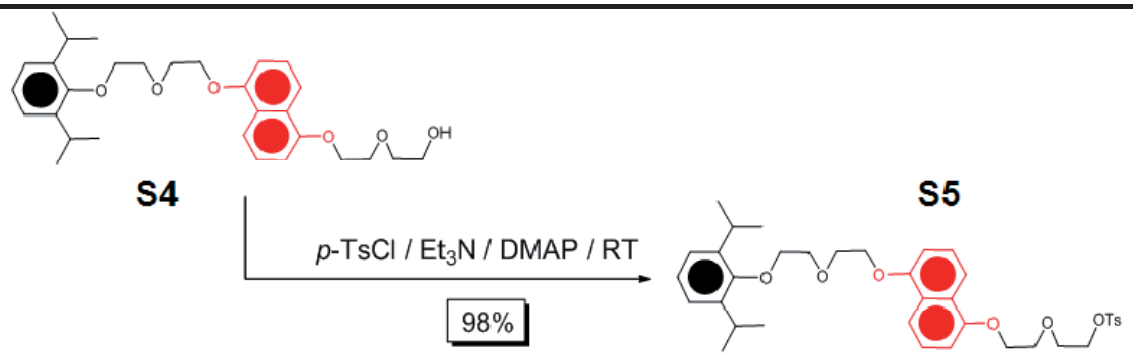

Scheme S5. Synthesis of DNP tosylate **S5**

S6: A solution of tosylate **S5** (1.5 g, 2.30 mmol) and NaN_3 (299 mg, 4.60 mmol) in dry DMF (15 mL) was heated at 80 °C for 20 h. After cooling, the solvent was removed in vacuo, and the crude material was filtered through a plug of silica, eluting with Me_2CO. A brown oil was obtained and found to be pure **S6** (1.24 mg, 98%). ^{1}H NMR (500 MHz, $CDCl_3$): δ = 8.00 (d, J = 8.5 Hz, 2H), 7.96 (d, J = 8.5 Hz, 2H), 7.43 (q, J = 8.5 Hz, 2H), 7.16 (s, 3H), 6.94 (d, J = 7.5 Hz, 1H), 6.90 (d, J = 7.5 Hz, 1H), 4.40 (t, J = 4.5 Hz, 2H), 4.33 (t, J = 4.5 Hz, 2H), 4.14 (t, J = 4.5 Hz, 2H), 4.05–4.01 (m, 6H), 3.84 (t, J = 4.5 Hz, 2H), 3.51–3.44 (m, 4H), 2.90 (d, J = 9.5 Hz, 2H), 1.29 (d, J = 7 Hz, 12H). ^{13}C NMR (125 MHz, $CDCl_3$): δ = 154.7, 154.5, 142.1, 127.1, 127.0, 125.5, 125.4, 124.9, 124.3, 115.0, 114.9, 106.0, 106.0, 74.3, 71.2, 70.6, 70.3, 70.1, 68.4, 68.2, 51.0, 26.5, 24.4. MS (ESI): *m/z* Calcd for $C_{30}H_{40}N_3O_5$: 522.29, found: 522.20 $[M + H]^+$.

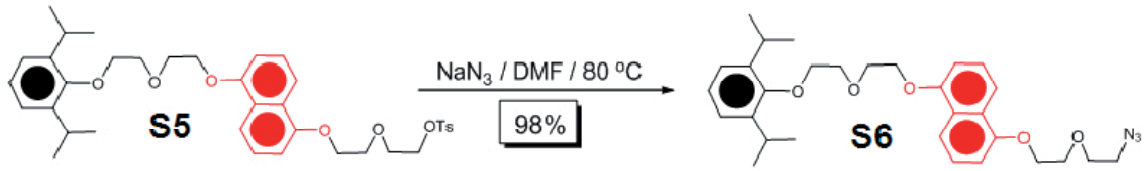

Scheme S6. Synthesis of DNP azide **S6**

0·2PF_6: The DNP azide **S6** (187.79 mg, 0.36 mmol), **V**·2PF_6 (400 mg, 0.72 mmol), and a catalytic amount of $Cu(MeCN)_4PF_6$ and TBTA were disolved in Me_2CO (10 mL) at room temperature. The reaction mixture was left to stir overnight. After removal of the solvent, the residue was redissolved in a minimal amount of Me_2CO, and a saturated aqueous solution of EDTA (pH 8) was added. Addition of NH_4PF_6 resulted in a precipitate, which, was collected by filtration and then further purified by column chromatography (SiO_2, Me_2CO plus 2% NH_4PF_6). The purple fractions were collected, concentrated to a minimum volume and **0**·2PF_6 was precipitated by the addition of H_2O. The precipitate was collected by filtration to afford **0**·2PF_6 (313.2 mg, 82%) as a red, glassy product. ^{1}H NMR (500 MHz, CD_3COCD_3): δ = 9.34 (d, *J* = 7.0 Hz, 2H), 9.20 (d, *J* = 7.0 Hz, 2H), 8.71 (d, *J* = 7.0 Hz, 2H), 8.66 (d, *J* = 7.0 Hz, 2H), 7.88 (s, 1H), 7.82 (d, *J* = 8.5 Hz, 1H), 7.68 (d, *J* = 8.5 Hz, 1H), 7.35 (d, *J* = 8.5 Hz, 1H), 7.32 (d, *J* = 8.0 Hz, 1H), 7.07 (m, 3H), 6.99 (d, *J* = 8.0 Hz), 6.90 (*J* = 8.0 Hz), 5.15 (t, *J* = 7.0 Hz, 2H), 5.05 (t, *J* = 7.0 Hz, 2H), 4.58 (t, *J* = 5.0 Hz, 2H), 4.36 (t, *J* = 4.4 Hz, 2H), 4.24 (t, *J* = 4.4 Hz, 2H), 4.07 (t, *J* = 4.4 Hz, 2H), 4.00-3.91 (m, 6H), 3.48 (t, *J* = 7.0 Hz, 2H), 3.44 (t, *J* = 7.0 Hz, 2H), 3.12 (d of t, J_d = 2.7 Hz, J_t = 6.5 Hz, 2H), 2.66 (t, *J* = 2.7 Hz, 1H), 1.14 (d, 7.0 Hz, 12H). ^{13}C NMR (125 MHz, CD_3COCD_3): δ = 155.2, 155.0, 153.9, 150.9, 150.5, 147.0, 146.9, 146.7, 142.4, 142.2, 127.6, 127.3, 127.3, 126.3, 126.1, 125.4, 124.7, 115.1, 115.0, 106.6, 106.5, 79.0, 75.0, 71.4, 70.5, 70.1, 70.0, 68.9, 68.5, 62.1, 60.8, 50.7, 27.7, 26.7, 24.3, 21.6. HRMS (HR-ESI): *m/z* Calcd for $C_{48}H_{56}F_6N_5O_5P$: 928.4043, found: 928.3989 $[M - PF_6]^+$. *m/z* Calcd for $C_{48}H_{57}N_5O_5$: 391.72, found: 391.70 $[M - 2PF_6]^{2+}$.

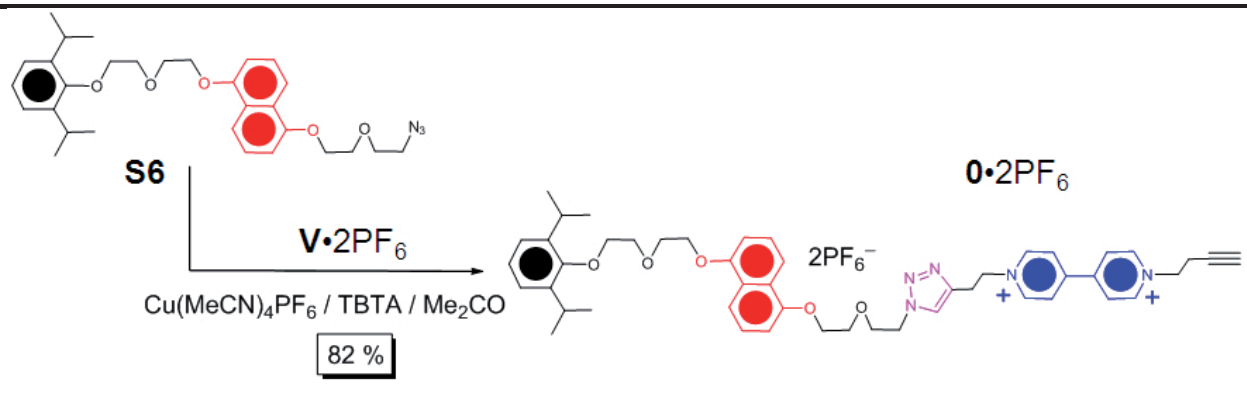

Scheme S7. Synthesis of DNP-**BIPY**$^{2+}$ derivative **0**·2PF_6

DB1·2PF_6: Compound **0**•2PF_6 (20 mg, 0.0186 mmol) and the azide **S2** (11 mg, 0.0378 mmol), along with a catalytic amount of $Cu(MeCN)_4PF_6$ and TBTA, were suspended in Me_2CO (10 mL) at room temperature. The reaction mixture was left to stir overnight. After removal of the solvent, the residue was redissolved in a minimal amount of Me_2CO, and a saturated aqueous solution of EDTA (pH 8) was added. Addition of NH_4PF_6 resulted in a precipitate, which was collected by filtration and further purified by column chromatography (SiO_2, Me_2CO plus 2% NH_4PF_6). The purple fractions were collected, concentrated to a minimum volume, and **DB1**·2PF_6 was precipitated by the addition of H_2O. The precipitate was collected by filtration to afford **DB1**·2PF_6 (85%) as a red, glassy product.

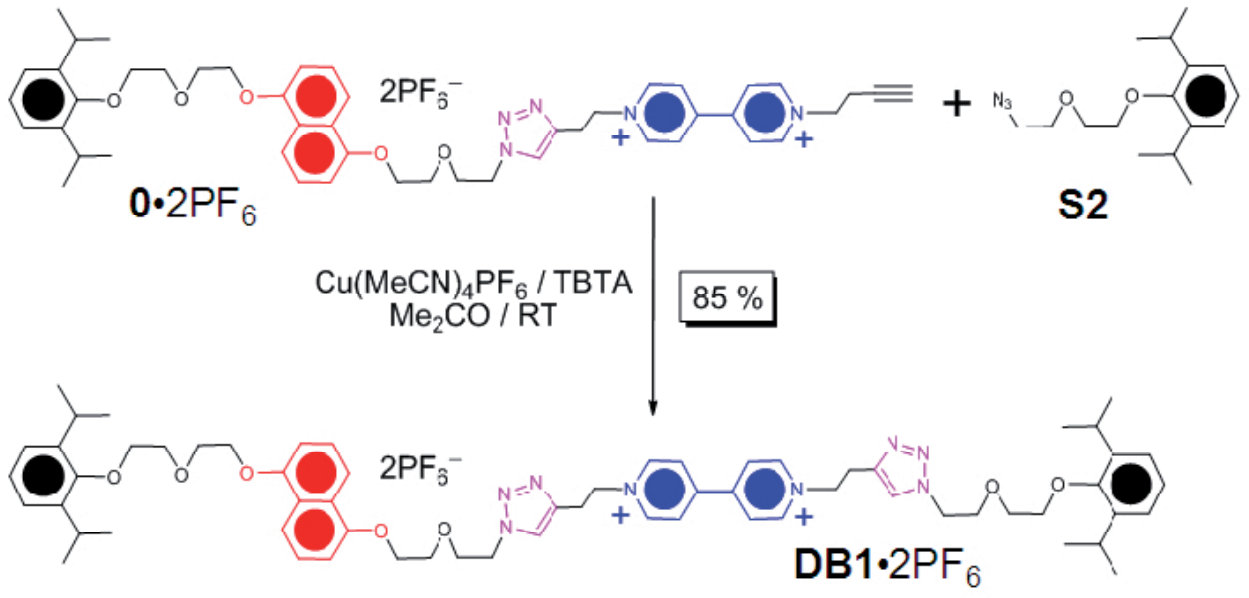

Scheme S8. Synthesis of the dumbbell **DB1**·2PF_6

^{1}H NMR (500 MHz, CD_3COCD_3): δ = 1.16 (d, *J* = 7 Hz, 12H), 1.17 (d. *J* = 7 Hz, 12H), 3.20 (q, 3H), 3.36 (septet, *J* = 7 Hz, 2H), 3.42–3.55 (m, 4H), 3.60 (t, *J* = 7 Hz, 2H), 3.82 (m, 2H), 3.87 (m, 2H), 3.92–4.06 (br m, 10H), 4.11 (br t, 2H), 4.26 (br t, 2H), 4.39 (br t, 2H), 4.60 (br m, 4H), 5.18 (t, *J* = 7 Hz, 2H), 5.24 (t, *J* = 7 Hz, 2H), 5.62 (s, 1H), 6.93 (d, *J* = 7 Hz, 1H), 7.03 (d, *J* = 7 Hz, 1H), 7.05–7.13 (m, 6H), 7.31–7.42 (m, 4H), 7.68–7.74 (m, 2H), 7.85 (d, *J* = 7 Hz, 1H), 7.90 (s, 2H), 8.66 (br d, 4H), 9.21 (d, *J* = 7 Hz, 2H), 9.28 (d, *J* = 7 Hz, 2H) ppm. ^{13}C NMR (125 MHz, CD_3COCD_3): δ = 14.6, 21.33, 24.36, 24.38, 26.8, 26.84, 27.78, 27.84, 42.9, 50.8, 50.9, 55.0, 62.1, 62.2, 68.7, 69.1, 70.1, 70.19, 70.21, 70.6, 71.0, 71.5, 74.7, 106.7, 106.8, 115.1, 115.2,

124.4, 124.5, 124.77, 124.81, 125.5, 125.6, 126.2, 126.4, 127.4, 127.5, 127.6, 127.7, 127.9, 130.5, 138.7, 142.3, 142.49, 142.54, 143.8, 147.02, 147.07, 150.6, 150.7, 153.9, 154.1, 155.2, 155.4 ppm. HRMS (HR-ESI): *m/z* Calcd for $C_{64}H_{81}F_6N_8O_7P$: 1219.5942, found: 1219.5993 $[M - PF_6]^+$. *m/z* Calcd for $C_{64}H_{81}N_8O_7$: 537.3171, found: 537.3115 $[M - 2PF_6]^{2+}$.

1·6PF_6: Compound **0**·2PF_6 (40 mg, 0.0372 mmol), **CBPQT**·4PF_6 (49 mg, 0.0446 mmol), and the azide **S2** were dissolved in Me_2CO (20 mL). The reaction was cooled down to 0 °C and left to stir overnight before adding catalytic amounts of $Cu(MeCN)_4PF_6$ and TBTA. The solution was then allowed to stir at 23 °C for 24 h. After removal of the solvent, the residue was redissolved in a minimal amount of Me_2CO, and a saturated aqueous solution of EDTA (pH 8) was added. Addition of NH_4PF_6 resulted in a precipitate, which was collected by filtration and further purified by column chromatography (SiO_2, Me_2CO plus 2% NH_4PF_6). Purple fractions were collected, concentrated to a minimum volume and **1**•6PF_6 was precipitated by the addition of H_2O. The precipitate was collected by filtration to afford a purple powder (72 mg, 79%).

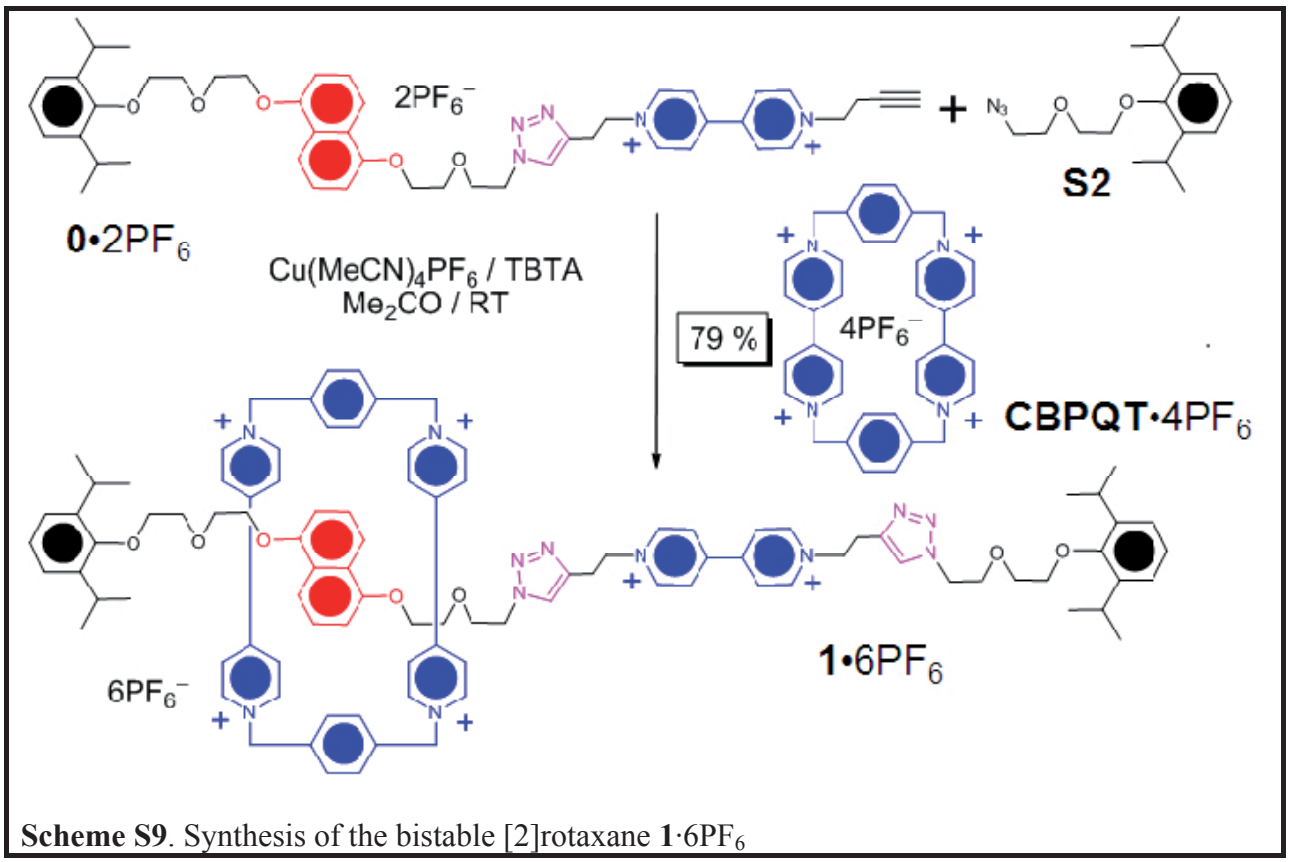

Scheme S9. Synthesis of the bistable [2]rotaxane **1**·6PF_6

^{1}H NMR (600 MHz, CD_3COCD_3, 243K): δ = 0.99 (br d, *J* = 7 Hz, 12H), 1.13 (d, *J* = 7 Hz, 12H), 2.65 (d, *J* = 8 Hz, 1H), 2.70 (d, *J* = 8 Hz, 1H), 3.64 (m, 4H), 3.81 (m, 10H), 3.95 (t, *J* = 5 Hz, 2H), 4.25 (br t, 4H), 4.33 (br s, 2H), 4.42 (br s, 4H), 4.52 (br d, 4H), 4.64 (t, *J* = 5 Hz, 2H), 4.84 (br t, 2H), 5.27 (m, 4H), 5.89 (d, *J* = 13 Hz, 2H), 6.08 (t, 4H), 6.21 (m, 4H), 6.38 (d, *J* = 8 Hz, 1H), 6.42 (d, *J* = 8 Hz, 1H), 7.06–7.18 (m, 7H), 7.36 (m, 8H), 7.72 (br d, 2H), 7.87 (m, 4H), 7.97 (m, 2H), 8.15 (s, 8H), 8.22 (s, 2H), 8.29 (s, 2H), 8.56 (s, 2H), 8.76 (d, *J* = 7 Hz, 2H), 8.79 (d, *J* = 7 Hz, 2H), 9.17 (d, *J* = 7 Hz, 2H), 9.20 (d, *J* = 7 Hz, 2H), 9.42 (m, 6H), 9.57 (d, *J* = 7 Hz, 2H) ppm. ^{13}C NMR (150 MHz, CD_3COCD_3, 243K): δ = 24.1, 24.2, 24.5, 25.9, 26.6, 26.7, 26.9, 30.9, 49.8, 65.4, 68.6, 71.1, 71.5, 105.3, 109.2, 124.6, 124.7, 125.1, 125.4, 125.7, 126.1, 127.2, 127.7, 129.1, 130.7, 131.3, 132.3, 137.6, 142.3, 142.4, 146.1, 146.2, 146.4, 151.9, 152.9, 153.6 ppm. HRMS (HR-ESI): *m/z* Calcd for $C_{100}H_{114}F_{30}N_{12}O_7P_5$: 2319.7137, found: 2319.7100 $[M - PF_6]^+$. *m/z* Calcd for $C_{100}H_{114}F_{24}N_{12}O_7P_4$: 1087.3750, found: 1087.3759 $[M - 2PF_6]^{2+}$.

S8: A solution of the tosylate[S10] **S7** (800 mg, 1.05 mmol) and NaN_3 (136.5 mg, 4.60 mmol) in dry DMF (15 mL) was heated at 80 °C for 20 h. After cooling down, the solvent was removed in vacuo, and the crude material was filtered through a plug of silica, eluting with Me_2CO. A yellow-brown oil was obtained and found to be pure **S8** (644 mg, 98%). ^{1}H NMR (500 MHz, $CDCl_3$): δ = 7.11 (s, 3H), 6.22 (d, *J* = 4.5 Hz, 2H), 4.33 (d, *J* = 19 Hz, 4H), 3.93 (t, *J* = 4.1 Hz, 2H), 3.87 (t, *J* = 5.1 Hz, 2H), 3.71 (t, *J* = 4.0 Hz, 2H), 3.71-3.68 (m, 6H), 3.66-3.64 (m, 2H), 3.42-3.35 (m, 4H), 1.23 (d, *J* = 6.9 Hz, 12H); ^{13}C NMR (125 MHz, $CDCl_3$): δ = 141.94, 134.73, 134.67, 134.54, 124.74, 124.12, 116.56, 116.43, 116.41, 116.34, 99.86, 73.94, 71.11, 70.80, 70.78, 70.25, 69.53, 69.49, 69.47, 68.48, 50.84, 26.37, 24.27. MS (ESI): *m/z* calcd for $C_{28}H_{39}N_3O_5S_4$: 625.18, found: 625.03.

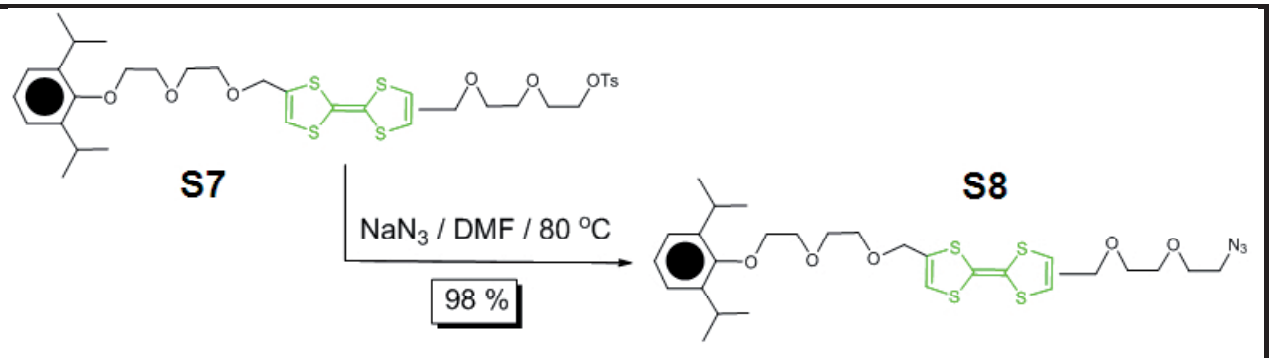

Scheme S10. Synthesis of the TTF azide **S8**

2·6PF_6: Compound **S8** (60 mg, 0.0958 mmol), **CBPQT**·4PF_6 (127 mg, 0.115 mmol), and **MSV**·2PF_6 (81 mg, 0.0961 mmol) were dissolved in Me_2CO (20 mL). The reaction was cooled down to 0 °C and left to stir overnight before adding a catalytic amounts of $Cu(MeCN)_4PF_6$ and TBTA. The solution was then allowed to stir at 23 °C for 24 h. After removal of the solvent, the residue was redissolved in a minimal amount of Me_2CO, and a saturated aqueous solution of EDTA (pH 8) was added. Addition of NH_4PF_6 resulted in a precipitate, which was collected by filtration and further purified by column chromatography (SiO_2: Me_2CO plus 2% ammonium hexafluorophosphate). Green fractions were collected, concentrated to a minimum volume and **2**·6PF_6 was precipitated by the addition of H_2O. The precipitate was collected by filtration to afford a green powder (128 mg, 52%).

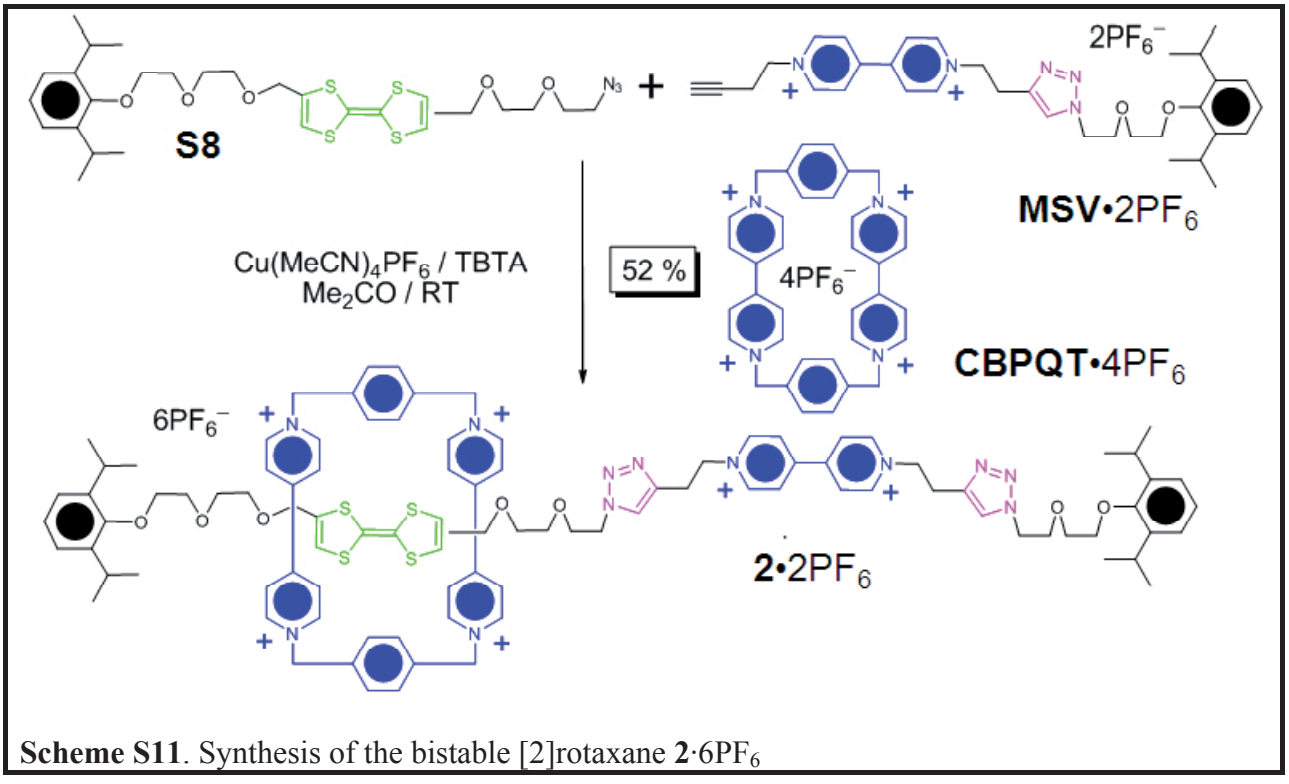

Scheme S11. Synthesis of the bistable [2]rotaxane **2**·6PF_6

^{1}H NMR (600 MHz, CD_3CN, 243K): δ = 1.08 (d, *J* = 7 Hz, 6H), 1.11 (d, *J* = 7 Hz, 12H), 2.07 (s, 6H), 2.93, (br m, 2H), 3.20–3.35 (br m, 4H), 3.40 (t, *J* = 7 Hz, 2H), 3.67–3.80 (br m, 14H), 3.86 (t, *J* = 7 Hz, 2H), 3.93–4.21 (br m, 6H), 4.52 (t, *J* = 5 Hz, 2H), 4.72 (t, *J* = 6 Hz, 1H), 4.93 (m, 2H), 5.53 (s, 8H), 5.57–5.71 (m, 4H), 6.05 (d, *J* = 15 Hz, 1H) 6.25 (d, *J* = 15 Hz, 1H), 7.02–7.12 (m, 5H), 7.27 (br d, 8H), 7.30–7.37 (m, 13H), 7.50 (d, *J* = 12 Hz, 1H), 7.55–7.76 (m, 6H), 7.80–7.95 (m, 7H), 8.25–8.31 (m, 2H), 8.33 (d, *J* = 7 Hz, 2H), 8.36 (d, *J* = 7 Hz, 2H), 8.71–8.80 (m, 1H), 8.83 (br d, 1H), 8.86 (br d, 1H), 8.91 (d, *J* = 7 Hz, 2H), 8.95 (d, *J* = 7 Hz, 1H), 8.97 (t, *J* = 7

Hz, 1H), 9.13 (d, J = 7 Hz, 1H), 9.15 (d, J = 7 Hz, 1H) ppm. ^{13}C NMR (150 MHz, CD_3CN): δ = 21.4, 24.1, 24.2, 26.4, 26.5, 27.5, 29.3, 30.8, 50.7, 54.0, 60.3, 61.5, 69.7, 70.6, 74.4, 74.7, 78.7, 124.4, 124.8, 124.9, 125.6, 125.8, 127.5, 127.6, 127.7, 128.6, 129.1, 129.6, 136.5, 142.0, 142.5, 146.37, 146.44, 146.5, 153.1 ppm. HRMS (HR-ESI): *m/z* Calcd for $C_{98}H_{114}F_{30}N_{12}O_7P_5S_4$: 2423.60198, found: 2423.60623 $[M - PF_6]^+$. *m/z* Calcd for $C_{98}H_{114}F_{24}N_{12}O_7P_4S_4$: 1139.32099, found: 1139.82133 $[M - 2PF_6]^{2+}$.

DB3·2PF$_6$ & 3·6PF$_6$ The procedure employed for the synthesis of the bistable [2]rotaxanes **1**·6PF$_6$ and **2**·6PF$_6$ were employed in the synthesis of the tristable rotaxane **3**·6PF$_6$ and its dumbbell **DB3**·2PF$_6$. The efficient and functional group tolerant ''Cu(I)-catalyzed azide/alkyne cycloaddition''[S11,S12] was utilized to obtain the final compounds **3**·6PF$_6$ and **DB3**·2PF$_6$ in 50 % and 49 % yields, respectively.

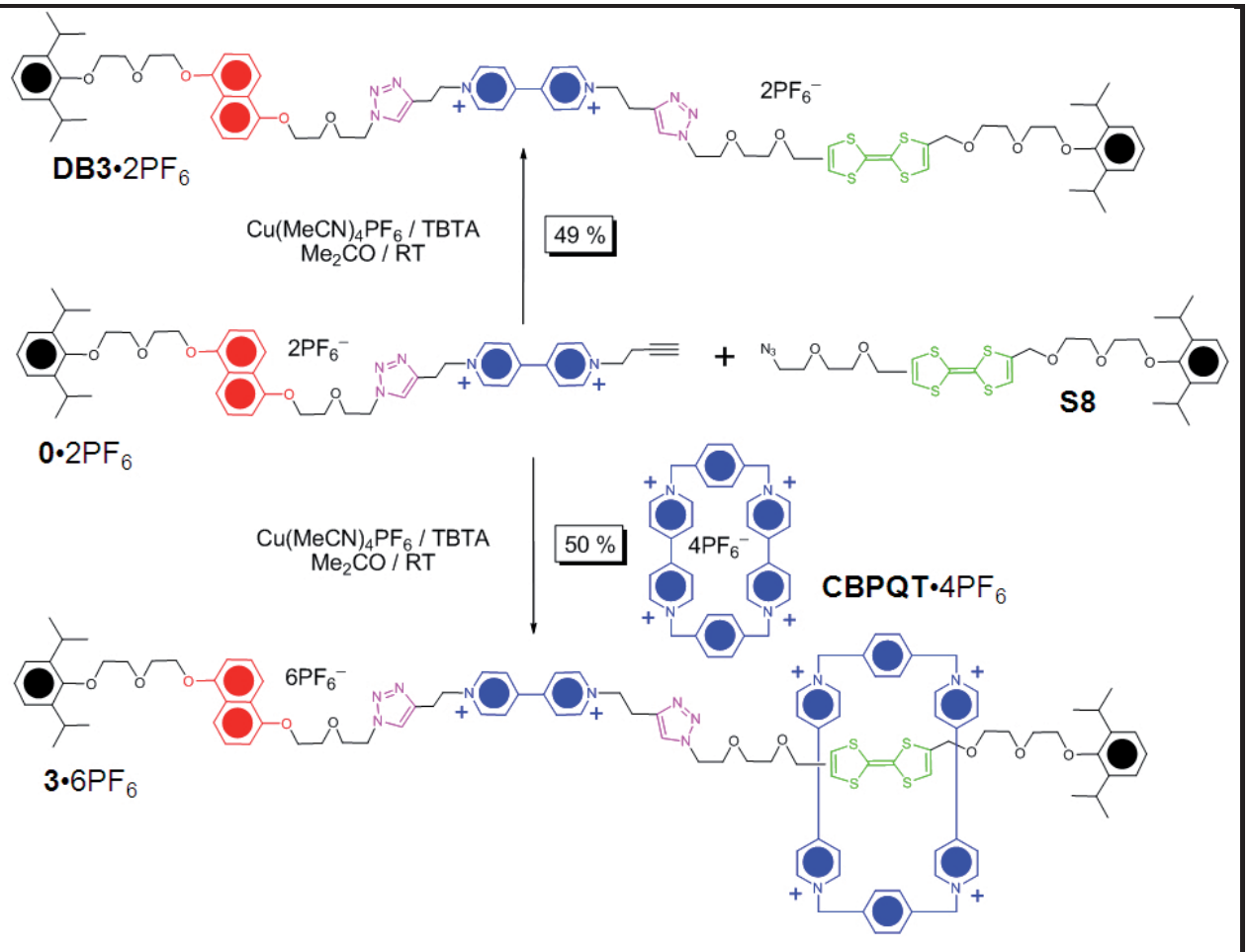

Scheme S12. Synthesis of the tristable TTF-viologen-DNP [2]rotaxane **3**·6PF$_6$ and its dumbbell **DB3**·2PF$_6$

3·6PF_6: ^{1}H NMR (600 MHz, CD_3CN, 243K) δ = 1.08 (br d, 24H), 3.21 (t, *J* = 7 Hz, 1H), 3.26-3.40 (m, 8H), 3.66 (br m, 1H), 3.71 (br m, 1H), 3.83 (m, 5H), 3.87-4.10 (m, 21H), 4.32 (br m, 3H), 4.55 (m, 3H), 4.58 (br t, 1H), 4.76 (t, *J* = 7 Hz, 1H), 4.80 (m, 3H), 5.32 (d, *J* = 13 Hz, 1H), 5.50-5.70 (m, 7H), 6.30 (d, 1H), 6.22 (s, 1H), 6.68 (t, *J* = 9 Hz, 1H), 6.88 (m, 1H), 7.02-7.15 (m, 8H), 7.18-7.30 (m, 3H), 7.45 (s, 1H), 7.48 (s, 1H), 7.53 (s, 3H), 7.62 (m, 3H), 7.66 (s, 1H), 7.69-7.80 (m, 8H), 7.84 (m, 1H), 7.90 (br t, 2H), 7.94 (m, 2H), 8.48 (d, *J* = 7 Hz, 1H), 8.51 (d, *J* = 7 Hz, 1H), 8.66 (br t, 2H), 8.79 (d, *J* = 7 Hz, 1H), 8.84-8.91 (m, 4H), 8.92 (d, *J* = 7 Hz, 1H), 9.04 (d, *J* = 6 Hz, 1H), 9.10 (d, *J* = 7 Hz, 1H) ppm. ^{13}C NMR (125 MHz, CD3CN, 298K) δ = 14.1, 14.7, 20.6, 20.6, 23.7, 26.2, 27.3, 27.4, 27.5, 28.0, 30.1, 32.7, 35.6, 35.7, 37.3, 50.9, 51.1, 51.3, 55.7, 59.6, 59.6, 59.6, 62.3, 62.5, 65.8, 68.7, 68.9, 69.1, 69.6, 70.4, 70.5, 70.6, 70.9, 71.3, 71.5, 71.6, 71.7, 71.8, 71.9, 75.0, 75.1, 75.4, 107.3, 115.4, 115.5, 120.8, 121.0, 124.9, 125.4, 125.6, 126.1, 126.3, 126.6, 126.9, 127.0, 127.7, 128.0, 128.1, 131.8, 132.1, 133.7, 134.6, 134.8, 137.1, 137.4, 142.7, 143.0, 143.2, 145.3, 145.8, 146.2, 146.6, 146.7, 147.0, 150.8, 154.1, 154.3, 155.4, 155.6 ppm. HRMS (HR-ESI): *m/z* Calcd for $C_{112}H_{128}F_{30}N_{12}O_{10}P_5S_4$: 2655.3775, found: 2655.7077 $[M - PF_6]^+$. *m/z* Calcd for $C_{112}H_{128}F_{24}N_{12}O_{10}P_4S_4$: 704.31, found: 704.30587 $[M - 2PF_6]^{2+}$.

DB3·2PF_6: ^{1}H NMR (600 MHz, CD_3CN, 243K): δ = 1.15 (m, 24H), 3.28–3.44 (m, 8H), 3.52 (m, 4H), 3.63 (m, 2H), 3.69 (m, 2H), 3.77 (m, 4H), 3.87 (m, 4H), 3.94 (m, 6H), 4.05 (m, 2H), 4.15 (br d, 2H), 4.19 (m, 2H), 4.28 (d, *J* = 5 Hz, 2H), 4.34 (m, 2H), 4.45 (m, 2H), 4.51 (m, 2H), 4.86 (m, 2H), 4.92 (m, 2H), 6.30 (s, 1H), 6.34 (d, *J* = 9 Hz, 1H), 6.88 (d, *J* = 7 Hz, 1H), 6.98 (d, *J* = 7 Hz, 1H), 7.05–7.13 (m, 6H), 7.33 (t, *J* = 8 Hz, 1H), 7.37 (t, *J* = 8 Hz, 1H), 7.67 (m, 3H), 7.79 (d, *J* = 8 Hz, 1H), 8.16 (m, 3H), 8.65 (d, 1H), 8.69 (br d, 1H) ppm. HRMS (HR-ESI): *m/z* Calcd for $C_{76}H_{96}F_6N_8O_{10}PS_4$: 1553.5827, found: 1553.57780 $[M - PF_6]^+$. *m/z* Calcd for $C_{76}H_{96}N_8O_{10}S_4$: 704.31135, found: 704.30587 $[M - 2PF_6]^{2+}$.

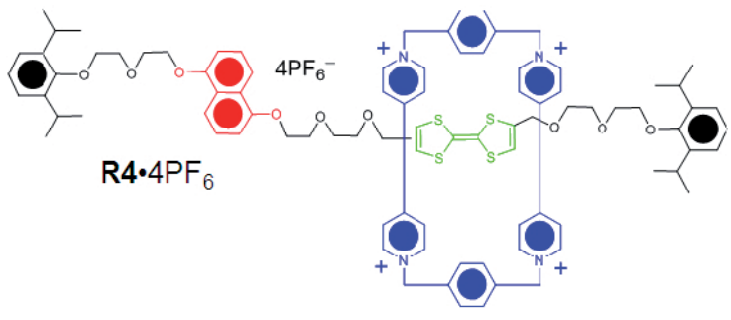

Scheme S13. Structure formula of the bistable [2]rotaxane $\mathbf{R}^{4+}$ used as a control for the EPR experiments. $\mathbf{R}^{4+}$ was synthesised according to literature procedures.[S10]

3. Cyclic Voltammetry (CV)

CV Experiments were performed by using a glassy carbon working electrode (0.018 cm^2, Cypress system). The electrode surface was polished routinely with 0.05 μm alumina-water slurry on a felt surface immediately before use. The counter electrode was a Pt coil and the reference electrode was a Ag/AgCl electrode. The concentrations of the sample and supporting electrolyte tetrabutylammonium hexafluorophosphate ($TBAPF_6$) were 1.0×10^{-3} mol L^{-1} and 0.1 mol L^{-1}, respectively. The scan rate was set to 200 mV s^{-1}.

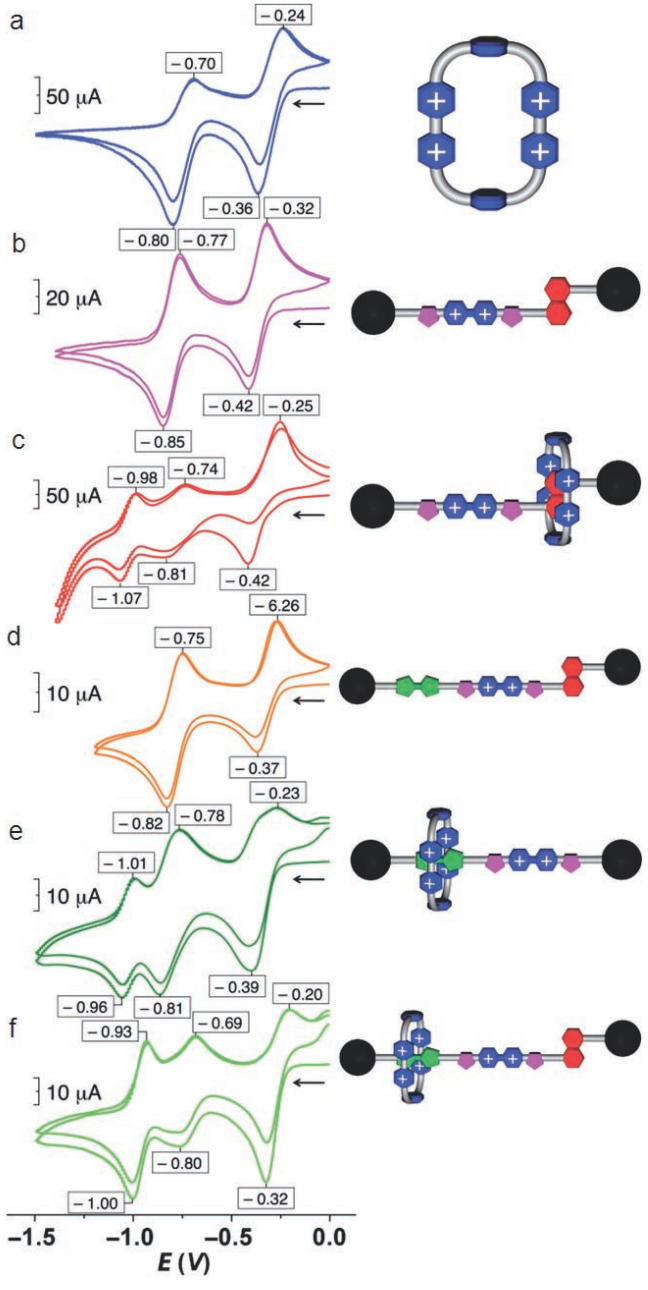

Figure S1: First and second CVs of **CBPQT**$^{2+}$ (**a**), dumbbells **DB1**·$2PF_6$ (**b**), **DB3**·$2PF_6$ (**d**), and [2]rotaxanes **1**·$6PF_6$ (**c**), **2**·$6PF_6$ (**e**) and **3**·$6PF_6$ (**f**). All the CVs were recorded under the same conditions of temperature (298 K), solvent (MeCN), concentrations (1 mM) and electrolyte (0.1 M $TBAPF_6$). The scan rate was set at 200 mV s^{-1}. CV Experiments were performed by using a glassy carbon working electrode (0.018 cm^2, Cypress system). The electrode surface was polished routinely with a 0.05 μm alumina-water slurry on a felt surface immediately before use. The counter electrode was a Pt coil and the reference electrode was a Ag/AgCl electrode. The values located in the rectangular boxes refer to selected reduction or oxidation peak potentials.

Typical cyclic voltammograms for **CBPQT**·4PF_6, and the dumbbells **DB1**·2PF_6 and **3**·2PF_6 are shown in **Figure S1**. While **CBPQT**·4PF_6 undergoes two consecutive reversible two-electron processes relative to the redox couples **CBPQT**$^{4+}$ / **CBPQT**$^{2(\bullet+)}$ and **CBPQT**$^{2(\bullet+)}$ / **CBPQT**^{0}, the two dumbbells, which contain a bipyridinium unit (**BIPY**$^{2+}$) in their structures, undergo two consecutive reversible one-electron processes. In the case of the rotaxanes **1**·6PF_6, **2**·6PF_6 and **3**·6PF_6, the second reduction peak of **BIPY**$^{2+}$ arising from the dumbbell and the **CBPQT**$^{4+}$ ring exhibits a large negative shift (100–150 mV), as well as separating into a set of two. These observations are in a good agreement with the formation of a stable inclusion complex, **BIPY**$^{\bullet+}$ ⊂ **CBPQT**$^{2(\bullet+)}$, as proposed in **Figure 1** in the main text. Shown in **Figure S2** are the CVs of the oxidative region for the [2]rotaxane **2**$^{6+}$ and its analogous dumbbell **DB3**$^{2+}$. The shift of the second oxidation peak of the **TTF** subunit is a consequence of the **CBPQT**$^{4+}$ ring remaining encircled around the **TTF**$^{\bullet+}$ radical cation formed after the first oxidation .

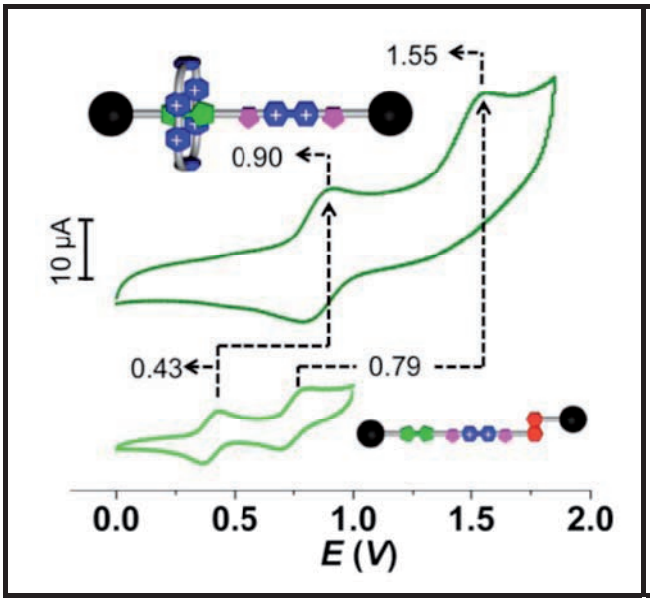

Figure S2: Cyclic voltammograms (MeCN / 0.1 M $TBAPF_6$ / 200 mV s^{-1}, second scans) of the rotaxane **2**$^{6+}$ and its analogous dumbbell **DB3**$^{2+}$. The values on the figure refer to the oxidation peak potentials.

Justification of the CV peak assignments for the equimolar mixture of CBPQT^{4+} and V^{2+} at 200 mV s^{-1}. In the case of the analysis using peak heights, one only needs to assume the diffusion coefficient of the complex **V**$^{\bullet+}$ ⊂ **CBPQT**$^{2(\bullet+)}$ does not change by a significant amount after the reduction process corresponding to the peak observed at –0.81 V (See Figure. 2e in the maintext). Likewise, using a convolutive semi-integrative technique, the same assumption about the diffusion coefficient must also be made. This assumption is reasonable to make considering that further reductions of the trisradical inclusion complex **V**$^{\bullet+}$ ⊂ **CBPQT**$^{2(\bullet+)}$ is not expected to

cause significant changes in its size. Both of the analytical methods reveal that the peak at –0.81 V corresponds to a one-electron process, which is assigned to the further reduction ($\mathbf{V}^{\bullet+} \subset \mathbf{CBPQT}^{2(\bullet+)} \rightarrow \mathbf{V}^{\bullet+} \subset \mathbf{CBPQT}^{(\bullet+)}$) of one of the bipyridinium radical cation units in the $\mathbf{CBPQT}^{2(\bullet+)}$ host not engaged in strong interactions with the $\mathbf{V}^{\bullet+}$ thread, while the reduction peak observed at –0.96 V corresponds to a two-electron process assigned to the simultaneous reductions of $\mathbf{V}^{\bullet+}$ and $\mathbf{CBPQT}^{(\bullet+)}$ to form the fully reduced $\mathbf{V}^{0} \subset \mathbf{CBPQT}^{0}$ complex. When the $\mathbf{CBPQT}^{4+}$ and $\mathbf{V}^{2+}$ are mixed together in MeCN and subjected to an applied potential of –0.7 V, the resultant UV/Vis spectrum displays absorption bands characteristic of dimer-type interactions. These bands are the result of the pimerization between *two* bypridinium radical cation units. Previous reports of viologen radical cation dimers have indicated[S13] that the dimers are EPR silent, whereas EPR data of the mixture of $\mathbf{CBPQT}^{4+}$ and $\mathbf{V}^{2+}$ subjected to a voltage of –0.7 V indicates the resultant species is EPR active. In addition, quantum mechanical calculations show that only one of the bipyridinium radical cation subunits of the $\mathbf{CBPQT}^{2(\bullet+)}$ is engaged in significant orbital overlap with the $\mathbf{V}^{\bullet+}$ thread. Taken together, these spectroscopic, EPR and theoretical data suggest that only one of the bipyridinium radical cation subunits of the $\mathbf{CBPQT}^{2(\bullet+)}$ is strongly interacting with the $\mathbf{V}^{\bullet+}$ radical cation at a given moment.

Formal thermodynamic analysis for the determination of the free energy of binding.

We first of all estimate the redox potential of the assigned two-electron oxidation process observed at 0 V at relatively fast scan rates corresponding to $\mathbf{V}^{\bullet+} \subset \mathbf{CBPQT}^{(\bullet+)(2+)} \rightarrow \mathbf{V}^{2+} \subset \mathbf{CBPQT}^{4+}$. Assuming Nernstian behaviour at ultrafast scan rates, the separation in voltage between anodic and cathodic peaks is given by the following expression: $\Delta E_p = 59/n$ mV, where ΔE_p is the separation between anodic and cathodic peak potentials and n is the number of electrons involved in the process. Having assigned the anodic peak at 0 V to a two-electron process, we calculate the separation to be 29.5 mV. Therefore the half-wave redox potential, given by the average value of the anodic and cathodic peaks is –14.75 mV, which we have subsequently rounded down to –10 mV (–0.1V).

Using Hess's law we can divide the reduction cycle represented by the redox ladder scheme shown in **Figure 5** in the main text into the following six individual one-electron processes, which, when summed, yield process (7):

$$\mathbf{CBPQT}^{(\bullet+)(2+)} = \mathbf{CBPQT}^{4+} + e^- \qquad -E_a \qquad (1)$$

$$\mathbf{CBPQT}^{2(\bullet+)} = \mathbf{CBPQT}^{(\bullet+)(2+)} + e^- \qquad -E_a \qquad (2)$$

$$\mathbf{V}^{\bullet+} = \mathbf{V}^{2+} + e^- \qquad -E_b \qquad (3)$$

$$\mathbf{V}^{\bullet+} \subset \mathbf{CBPQT}^{(\bullet+)(2+)} = \mathbf{V}^{\bullet+} \subset \mathbf{CBPQT}^{2(\bullet+)} - e^- \qquad E_c \qquad (4)$$

$$\mathbf{V}^{\bullet+} \subset \mathbf{CBPQT}^{4+} = \mathbf{V}^{\bullet+} \subset \mathbf{CBPQT}^{(\bullet+)(2+)} - e^- \qquad E_d \qquad (5)$$

$$\mathbf{V}^{2+} + \mathbf{CBPQT}^{4+} = \mathbf{V}^{\bullet+} \subset \mathbf{CBPQT}^{4+} - e^- \qquad E_d \qquad (6)$$

$$\mathbf{V}^{\bullet+} + \mathbf{CBPQT}^{2(\bullet+)} = \mathbf{V}^{\bullet+} \subset \mathbf{CBPQT}^{2(\bullet+)} \qquad K_f \qquad (7)$$

Using the Nernst equation we can then derive the following equation:

$$-\Delta G(K_f) = nFE_a + nFE_b + nFE_b - nFE_c - nFE_d - nFE_d \qquad [1]$$

Upon rearranging the terms, we obtain:

$$-\Delta G(K_f) = nF(E_a - E_c) + nF(E_a - E_d) + nF(E_b - E_d) \qquad [1a]$$

And using a more concise notation, we can write:

$$-\Delta G(K_f) = nF\Delta E_{a-c} + nF\Delta E_{a-d} + nF\Delta E_{b-d} \qquad [1c]$$

where n = 1 on account of the fact that the processes (1)–(6) all represent one-electron redox processes, and F is Faraday's constant. Using equation [1] we calculate $\Delta G(K_f) = -17$ kcal mol^{-1}, which agrees well with the binding energy predicted from the theoretical quantum mechanical calculations.

4. Spectroelectrochemistry (SEC)

SEC Experiments were made in a custom-built optically-transparent thin-layer electrochemical (OTTLE) cell with an optical path of 1 mm (2 mm), using a Pt grid as working electrode, a Pt wire as counter electrode and a Ag wire pseudo-reference electrode. Experimental errors: potential values, +/– 10 mV; absorption maxima, +/– 1 nm. UV/Vis Spectra were recorded in MeCN at room temperature on a Varian 100 Bio-instrument.

1·6PF$_6$ & DB1·2PF$_6$. The bistable rotaxane **1**·6PF$_6$ was designed to switch only under reducing conditions. The ground state (E = 0 V) UV/Vis spectrum (**Figure S3**) of **1**·6PF$_6$ displays the characteristic charge transfer (CT) band at 529 nm, corresponding to the CT interaction between the DNP unit and the **CBPQT**$^{4+}$ ring. The absorption spectrum starts to change on applying a potential of –0.7 V, and new bands at 536 nm and 1075 nm start to appear, characteristic of the formation of a **BIPY**$^{\bullet+}$ radical cation dimer, which for these mechanically bonded systems indicates the encirclement of the **CBPQT**$^{2(\bullet+)}$ around the bipyridinium radical cation unit of the dumbbell. The spectrum gradually changes back to its original form when the applied potential is switched off (E = 0 V), or when the sample is exposed to oxygen, indicating that all the electrochemical redox processes undergone by **1**·6PF$_6$ are fully reversible. In the case of the dumbbell **DB1**·2PF$_6$ where no **CBPQT**$^{4+}$ ring is present, applying a voltage of –0.7 V results in characteristic bands of a non-dimer viologen radical cation (604 nm).

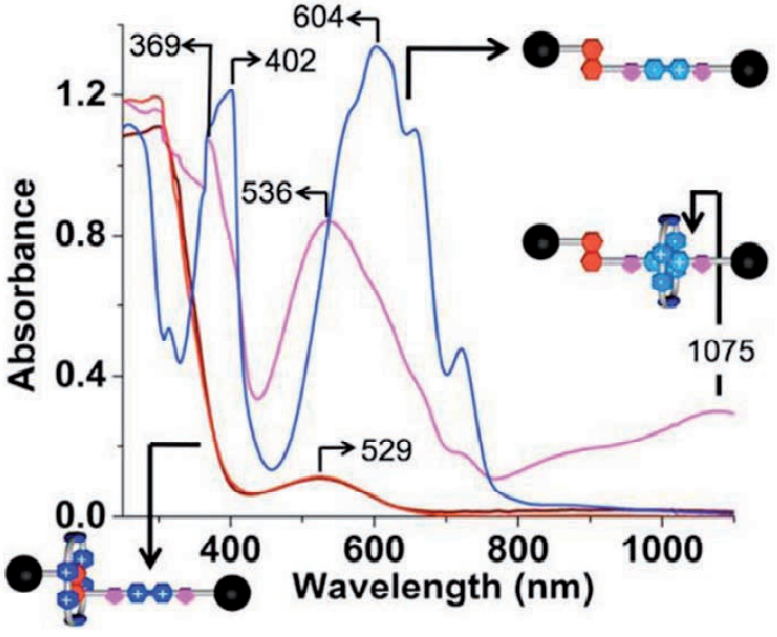

Figure S3: The changes in the UV/Vis spectra during the SEC measurements conducted on the [2]rotaxane **1**·6PF$_6$ and its dumbbell **DB1**·2PF$_6$. The applied potential changes from E = 0 (red for **1**·6PF$_6$), to –0.7 V (purple for **1**·6PF$_6$ and blue for **1**·2PF$_6$). All data were recorded in Ar purged MeCN (0.1 M TBAPF$_6$) at 298 K. The concentrations of the samples were 1.0 mM.

2·6PF$_6$. The bistable rotaxane **2**·6PF$_6$ can be switched under both reduction and oxidation conditions (**Figure S4**). The ground state (E = 0 V) UV/Vis spectrum of **2**·6PF$_6$ displays the characteristic CT band at 840 nm, corresponding to the CT interaction between the TTF unit and the **CBPQT**$^{4+}$ ring. The absorption spectrum starts to change on applying a potential of +0.9 V, the ground state bands bleach and new absorption bands emerge at λ_{max} = 445 and 595 nm, which correspond to the TTF$^{+\bullet}$ radical cation. When the applied potential is increased above +1.5 V, the absorption bands of the TTF$^{+\bullet}$ radical cation on its own begins to bleach and a new peak (λ_{max} = 380 nm) emerges for the TTF^{2+} dication. Since the DNP site was omitted from the structure of the dumbbell and replaced by the **BIPY**$^{2+}$ unit, no absorption peak at 525 nm associated with the CT band between the DNP unit and the **CBPQT**$^{4+}$ ring can be detected, and the **CBPQT**$^{4+}$ ring is hypothesized to shuttle back and forth along the dumbbell axis with no preferences. Returning the system to zero bias (E = 0 V) reduces the TTF^{2+} dication back to its neutral state (TTF). The spectrum gradually changes back to its original form when the sample is left at room temperature for 12 h, indicating that all the electrochemical redox processes undergone by **2**·6PF$_6$ are fully reversible. Moreover, the **2**·6PF$_6$ rotaxane can also be switched under reducing conditions. As described for **1**·6PF$_6$, applying a potential of –0.7 V results in the appearance of new bands at 540 and 1075 nm characteristic of the formation of a **BIPY**$^{\bullet+}$ radical cation dimer, and indicative of the encirclement of the **CBPQT**$^{2(\bullet+)}$ around the bipyridinium radical cation unit of the dumbbell. Again, when the applied potential is switched off (E = 0 V) or the sample is exposed to oxygen, the original spectrum of the ground state co-conformation (GSCC) is recovered.

3·6PF$_6$ & DB3·2PF$_6$. The tristable rotaxane **3**·6PF$_6$ can also be switched under both reduction and oxidation conditions (**Figure S5**). While the transition from the TTF to the DNP unit occurs after oxidation of the TTF, the transition to the bipyridinium unit occurs only under reduction conditions. In the TTF→DNP migration, Coulombic forces arising from the **BIPY**$^{2+}$ act to accelerate the transition from the oxidised TTF to the DNP unit. The ground state (E = 0 V) UV/Vis spectrum of **3**·6PF$_6$ displays the characteristic CT band at 846 nm, corresponding to the CT interaction between the TTF unit and the **CBPQT**$^{4+}$ ring. The absorption spectrum starts to

change on applying a potential of +1.0 V. The ground state bands bleach and new absorption bands emerge at λ_{max} = 380 nm corresponding to the TTF^{2+} dication. The bleaching of the CT band around 840 nm indicates that the **CBPQT**$^{4+}$ ring has moved away from the oxidized TTF to the DNP unit.

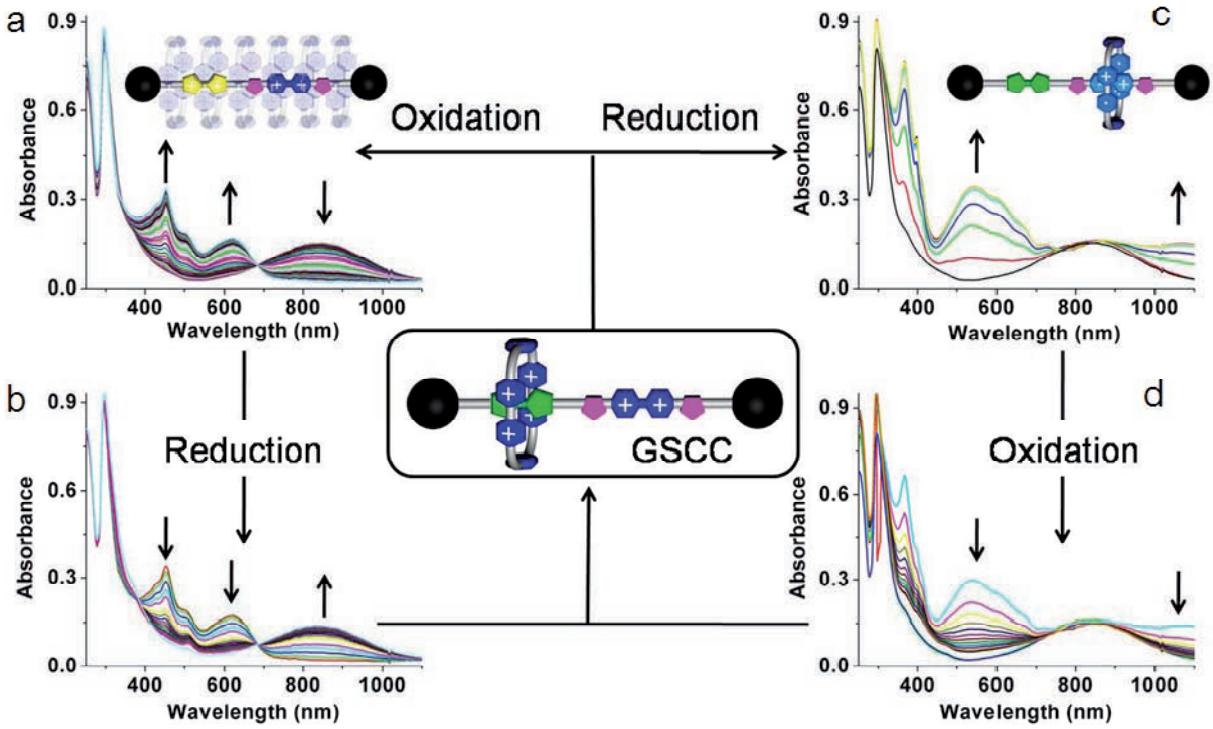

Figure S4: The changes in the UV/Vis spectra during the SEC measurements conducted on the [2]rotaxane **2**·6PF_6. (**a**) The applied potential changes from E = 0, to +0.8 V. (**b**) The potential was set back to 0 V and the initial spectrum was recovered. (**c**) The applied potential changes from E = 0, to –0.7 V. (**d**) Back to 0 V, the initial spectrum was recovered. All data were recorded in Ar purged MeCN (0.1 M $TBAPF_6$) at 298 K. The concentrations of the samples were 1.0 mM.

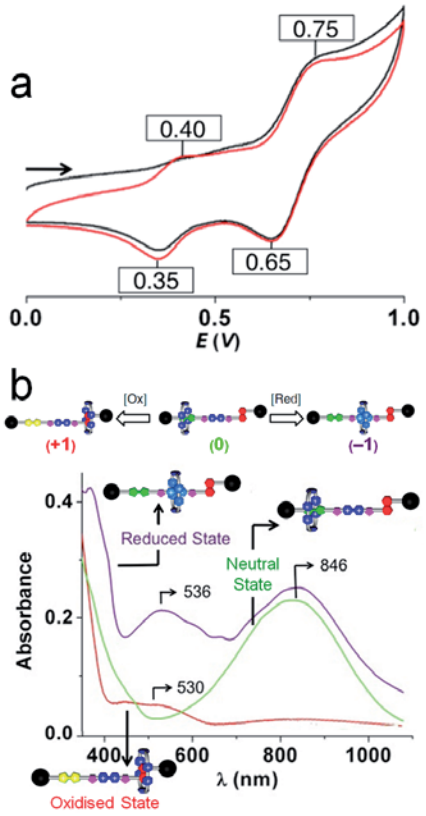

Figure S5: (**a**) First and second CVs of the [2]rotaxane **3**·6PF$_6$ in the oxidation region showing a typical voltammogram of a TTF/DNP based [2]rotaxane. (**b**) The changes in the UV/Vis spectra during the SEC measurements conducted on the [2]rotaxane **3**·6PF$_6$. The applied potential changes from E = 0 to +0.8 V. The potential was set back to 0 V and the initial spectrum was recovered. The applied potential changes from E = 0 to –0.7 V. Back to 0 V and the initial spectrum was recovered. All data were recorded in Ar purged MeCN (0.1 M TBAPF$_6$) at 298 K. The concentrations of the samples and supporting electrolyte were 1.0 mM and 0.1 M, respectively.

At E = +1.22 V, a small absorption peak at around 530 nm associated with the CT band between DNP and **CBPQT**$^{4+}$ can be detected. Returning the system to zero bias (E = 0 V) will reduce the TTF^{2+} dication back to its neutral state (TTF). The spectrum gradually changes back to its original form when the sample is left at room temperature for 12 h, indicating that all the electrochemical redox processes undergone by **3**·6PF$_6$ are fully reversible. Moreover, the rotaxane **3**·6PF$_6$ can also be switched under reduction conditions. Applying a potential of –0.7 V results in the appearance of new bands at 580 and 900 nm characteristic of the formation of a **BIPY**$^{\bullet+}$ radical cation dimer, indicative of the encirclement of the **CBPQT**$^{2(\bullet+)}$ around the bipyridinium radical cation unit of the dumbbell. Again, when the applied potential is switched off (E = 0 V) or the sample is exposed to oxygen, the original spectrum (GSCC) is recovered. For comparison sake, the SEC of the **DB3**·2PF$_6$ dumbbell has also been recorded under the same conditions, and shows only the formation of the viologen radical cation.

Density Functional Theory (DFT)

Density functional theory (DFT) has been a useful computational tool[S14,S15,S16,S17] for the designing and understanding of mechanically interlocked molecules (MIMs). Especially, the newly developed M06-class[S18] of density functionals has been shown[S19] to provide a better description for the structural, optical and binding properties of MIMs and their precursor complexes. Here, we use the M06 flavor of DFT to predict the binding in the $\mathbf{V}^{\bullet+} \subset \mathbf{CBPQT}^{2(\bullet+)}$ superstructure as well as the fully reduced complex $\mathbf{V}^{0} \subset \mathbf{CBPQT}^{0}$ (**Table S1**). **Table S2** shows the energetic differences between the doublet and quartet multiplicities for the inclusion complex $\mathbf{MV}^{\bullet+} \subset \mathbf{CBPQT}^{2(\bullet+)}$ $[PF_6]_3$. The minimised superstructures for $\mathbf{MV}^{\bullet+} \subset \mathbf{CBPQT}^{2(\bullet+)}$ $[PF_6]_3$ and the fully reduced complex are shown in **Figure S6**.

Table S1. Detailed computational energetics of the inclusion complex $\mathbf{MV}^{\bullet+} \subset \mathbf{CBPQT}^{2(\bullet+)}$ $[PF_6]_3$ and the fully reduced $\mathbf{MV} \subset \mathbf{CBPQT}$.

Complex	Charge	Total Multiplicity	Single Point Gas Phase M06/6-311++G**	M06/6-31G** Acetonitrile	CP correction
			E_{SCF}	Vsolv	Kcal/mol
$\mathbf{CBPQT}^{2(\bullet+)}$ $\mathbf{[PF_6]_2}$	0	S=1	−3489.65958534	−45.15	5.6
$\mathbf{MV}^{\bullet+}$ $\mathbf{[PF_6]}$	0	S=1/2	−1515.456476	−28.55	
$\mathbf{MV}^{\bullet+} \subset \mathbf{CBPQT}^{2(\bullet+)}$ $\mathbf{[PF_6]_3}$	0	S=1/2	−5005.94056	−54.70	
Complex	**Charge**	**Total Multiplicity**	**Single Point Gas Phase M06/6-311++G****	**M06/6-31G** Acetonitrile**	**CP correction**
			E_{SCF}	Vsolv	Kcal/mol
CBPQT	0	S=0	−1609.179053	−15.65	4.5
MV	0	S=0	−574.8539103	−9.27	
$\mathbf{MV} \subset \mathbf{CBPQT}$	0	S=0	−2184.072661	−17.26	

Table S2. Energetic comparison of the doublet and quartet multiplicities for the inclusion complex $\mathbf{MV}^{\bullet+} \subset \mathbf{CBPQT}^{2(\bullet+)}$ $[PF_6]_3$.

Complex	charge	Multiplicity	M06/6-31G**
$\mathbf{MV}^{\bullet+} \subset \mathbf{CBPQT}^{2(\bullet+)}$ $\mathbf{[PF_6]_3}$	0	S=1/2	−5004.92394374
$\mathbf{MV}^{\bullet+} \subset \mathbf{CBPQT}^{2(\bullet+)}$ $\mathbf{[PF_6]_3}$	0	S=3/2	−5004.93649299

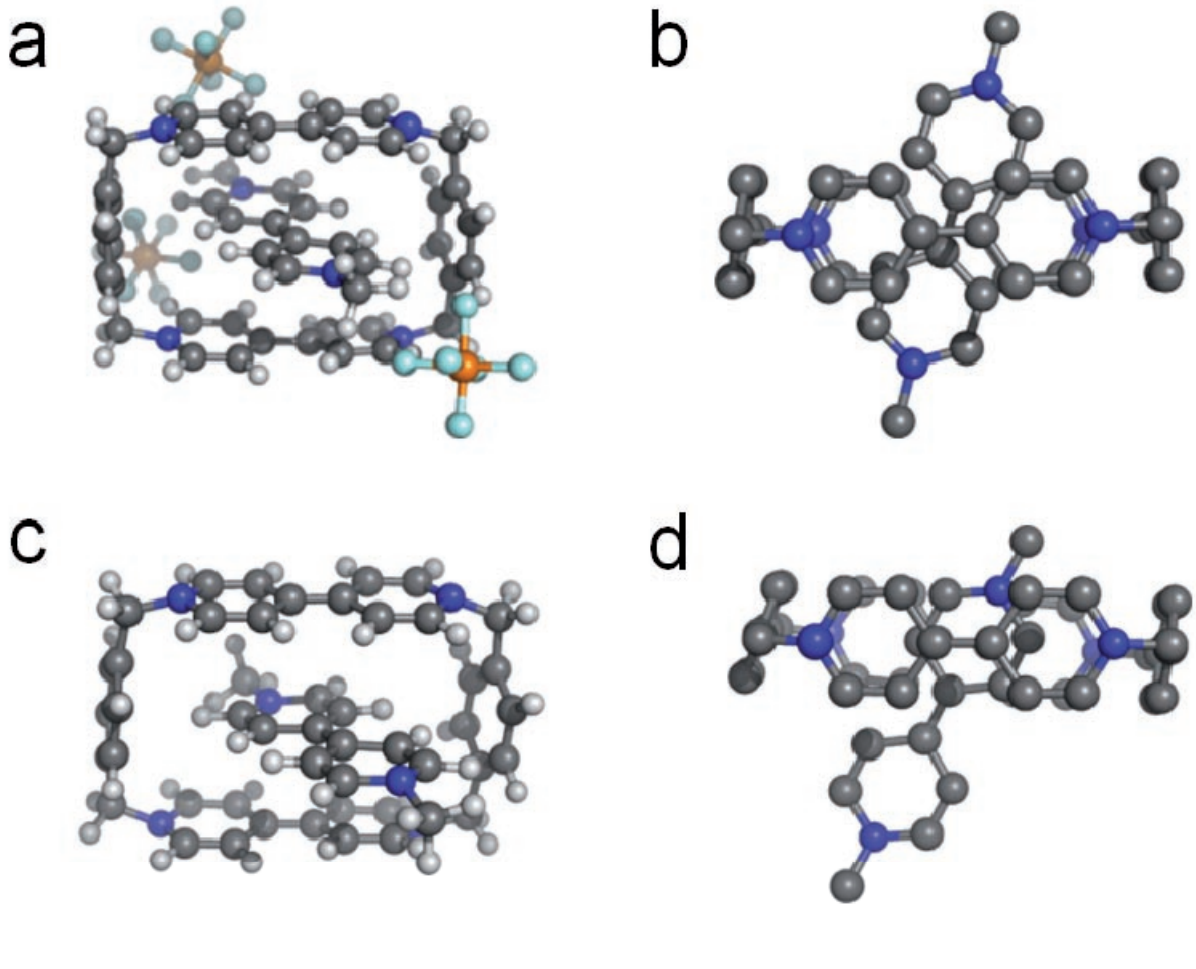

Figure S6. Calculated minimized superstructures (side-view) (**a**) / (**c**) and (top-view) (**b**) / (**d**) for the inclusion complex $\mathbf{V}^{\bullet+} \subset \mathbf{CBPQT}^{2(\bullet+)}$ and the fully reduced complex $\mathbf{V}^{0} \subset \mathbf{CBPQT}^{0}$, respectively.

5. Electron Paramagnetic Resonance (EPR)

Transient nutation (**Figure S7**) is a technique, which can determine the spin multiplicity of a system by comparing the nutation frequency of the sample in question to the nutation frequency of a sample with a known spin multiplicity. BDPA's is known to be spin ½. Since all samples presented here match BDPA's frequency of 26 MHz, we conclude that they are also spin ½ systems. This observation indicates that, although we are in the fast exchange regime, the orbital overlap is not substantial enough to result in a change in spin multiplicity. **Figure S8** displays the steady state CW EPR of a 1:1 mixture of $\mathbf{CBPQT}^{2(\bullet+)}$ ring and the dumbbell $\mathbf{DB1}^{\bullet+}$. The CW

EPR spectrum exhibits the superposition of the spectra of dumbbell **DB1**$^{\bullet+}$ and **CBPQT**$^{2(\bullet+)}$ alone (see main text: **Figure 7**), an observation which indicates the lack of intermolecular interactions between the two combined species.

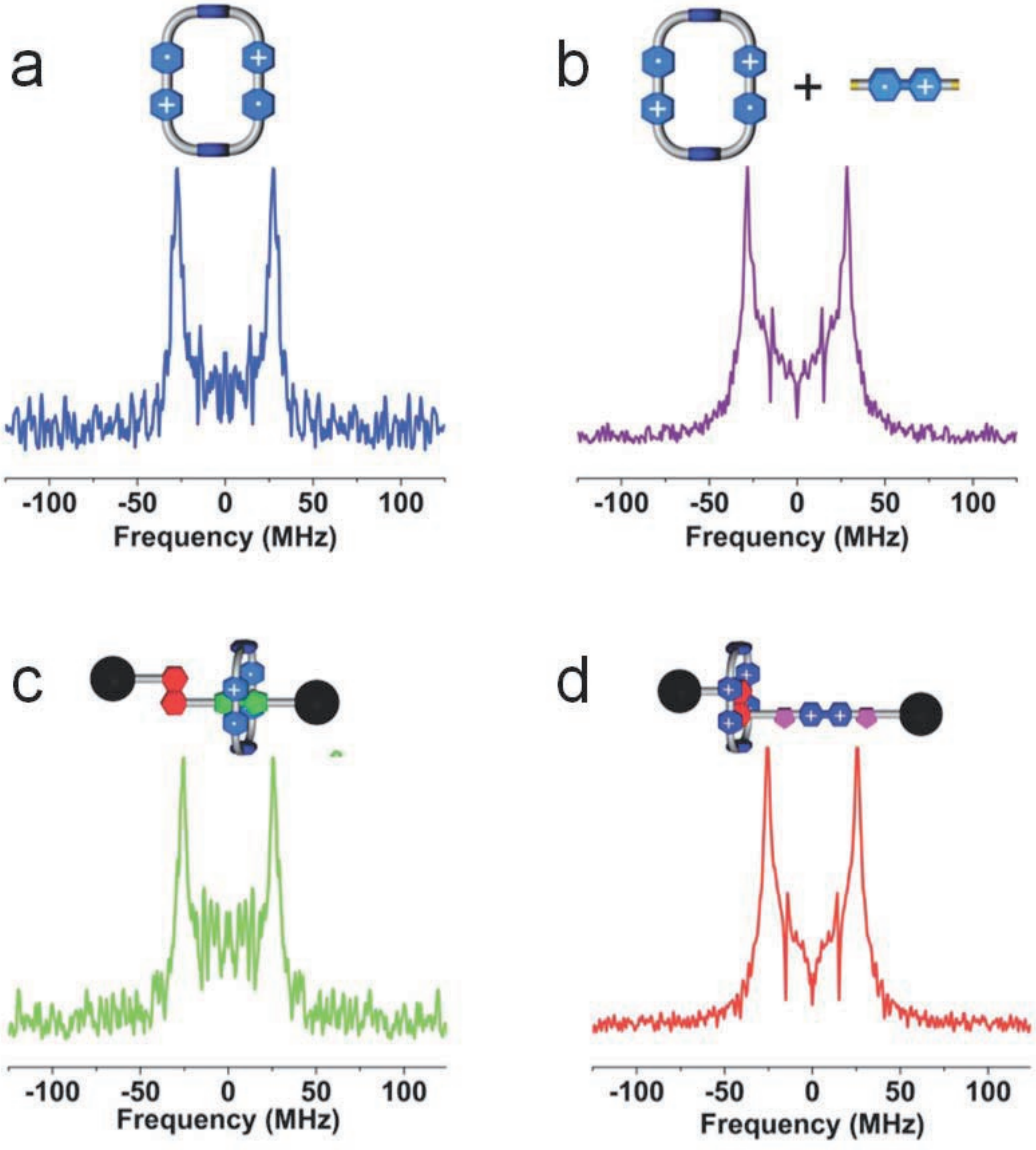

Figure S7: FT of transient nutation spectra of (**a**) **CBPQT**$^{2(\bullet+)}$, b) 1:1 mixture of **CBPQT**$^{2(\bullet+)}$ and **V**$^{\bullet+}$, (**c**) rotaxane **R**$^{2(\bullet+)}$, and (**d**) rotaxane **1**$^{2(\bullet+)}$.

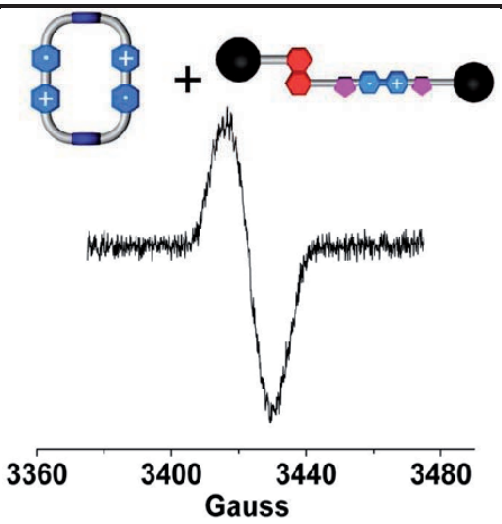

Figure S8: Steady-state CW EPR of a 1:1 mixture of **CBPQT**$^{2(\bullet+)}$ and the dumbbell **DB1**$^{\bullet+}$ showing the lack of intermolecular interactions between the two combined. The CW EPR spectrum exhibits the superposition of the spectra of dumbbell **DB1**$^{\bullet+}$ and **CBPQT**$^{2(\bullet+)}$ alone. These spectra were recorded in MeCN at room temperature. Concentration used for samples is ~10^{-3}M.

6. Additional References

S1. Asakawa, M., Brown, C.L., Pasini, D., Stoddart, J.F. & Wyatt, P. G. Enantioselective recognition of amino acids by axially-chiral π-electron-deficient receptors. *J. Org. Chem.* **61,** 7234–7235 (1996).

S2. Trabolsi, A. *et al.* Redox-driven switching in pseudorotaxanes. *New J. Chem.* **33,** 254–263 (2009).

S3. Saha, S. *et al.* A redox-driven multicomponent molecular shuttle. *J. Am. Chem. Soc.* **129,** 12159–12171 (2007).

S4. Nguyen, T.D. *et al.* Design and optimization of molecular nanovalves based on redox-switchable bistable rotaxanes. *J. Am. Chem. Soc.* **129,** 626–634 (2007).

S5. Nygaard, S. *et al.* Functionally rigid bistable [2]rotaxanes. *J. Am. Chem. Soc.* **129,** 960–970 (2007).

S6. Ashton, P.R. *et al.* Self-assembly, spectroscopic, and electrochemical properties of [n]rotaxanes. *J. Am. Chem. Soc.* **118,** 4931–4951 (1996).

S7. Collier, C.P. *et al.* Molecular-based electronically switchable tunnel junction devices. *J. Am. Chem. Soc.* **123,** 12632–12641 (2001).

S8. Chan, T.R., Hilgraf, R., Sharpless, K.B. & Fokin V.V. Polytriazoles as copper(I)-stabilizing ligands in satalysis. *Org. Lett.* **6,** 2853–2855 (2004).

S9. Saha, S. *et al.* A redox-driven multicomponent molecular shuttle. *J. Am. Chem. Soc.* **129,** 12159–12171 (2007).

S10. Brough, B. *et al.* Evaluation of synthetic linear motor-molecule actuation energetics. *Proc. Natl. Acad. Sci. USA* **103,** 8583–8588 (2006).

S11. Rostovtsev, V.V., Green, L.G., Fokin, V.V. & Sharpless, K.B. A stepwise Huisgen cycloaddition process: Copper(I)-catalyzed regioselective "ligation" of azides and terminal alkynes. *Angew. Chem., Int. Ed.* **41,** 2596–2599 (2002).

S12. Tornoe, C.W., Christensen, C. & Meldal, M. Peptidotriazoles on solid phase: [1,2,3]-triazoles by regiospecific copper(I)-catalyzed 1,3-dipolar cycloadditions of terminal alkynes to azides. *J. Org. Chem.* **67,** 3057–3064 (2002).

S13. Evans, A.G., Evans, J.C. & Baker, M.W. Electron spin resonance study of the dimerization equilibrium of the radical cation of 1,1'-diethyl-4,4'-bipyridylium diiodide in methanol. *J. Am. Chem. Soc.* **99,** 5882–5884 (1977).

S14. Deng, W.Q., Flood, A.H., Stoddart, J.F. & Goddard, W.A. An electrochemical color-switchable RGB dye: tristable [2]catenane. *J. Am. Chem. Soc.* **127,** 15994–15995 (2005).

S15. Jang, Y.H. & Goddard, W.A. Mechanism of oxidative shuttling for [2]rotaxane in a Stoddart-Heath molecular switch: Density functional theory study with continuum-solvation model. *J. Phys. Chem. B* **110,** 7660–7665 (2006).

S16. Kim, Y.H. & Goddard, W.A. Efficiency of pi-pi tunneling in [2]rotaxane molecular electronic switches. *J. Phys. Chem. C* **111,** 4831–4837 (2007).

S17. Ikeda, T. *et al.* Toward electrochemically controllable tristable three-station [2]catenanes. *Chem. Asian J.* **2,** 76–93 (2007).

S18. Zhao, Y. & Truhlar, D. G. The M06 suite of density functionals for main group thermochemistry, thermochemical kinetics, noncovalent interactions, excited states, and transition elements: two new functionals and systematic testing of four M06-class functionals and 12 other functionals. *Theoretical Chemistry Accounts* **120,** 215–241 (2008).

S19. Benitez, D., Tkatchouk, E., Yoon, I.I., Stoddart, J.F. & Goddard, W.A. Experimentally-based recommendations of density functionals for predicting properties in mechanically interlocked molecules. *J. Am. Chem. Soc.* **130,** 14928–14929 (2008).